Dysregulated expression of cholesterol biosynthetic genes in Alzheimer's disease alters epigenomic signatures of hippocampal neurons

I. Paiva, J. Seguin, I. Grgurina, A. K. Singh, B. Cosquer, D. Plassard, L. Tzeplaeff, S. Le Gras, Ludovica Cotellessa, C. Decraene, et al.

Neurobiology of Disease 198 (2024) 106538

Contents lists available at ScienceDirect

Neurobiology of Disease

journal homepage: www.elsevier.com/locate/ynbdi

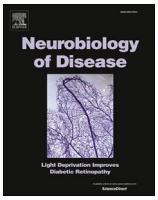

Dysregulated expression of cholesterol biosynthetic genes in Alzheimer's disease alters epigenomic signatures of hippocampal neurons

Isabel Paiva [a,b,*,1], Jonathan Seguin [a,b], Iris Grgurina [a,b], Akash Kumar Singh [c], Brigitte Cosquer [a,b], Damien Plassard [d], Laura Tzeplaeff [a,b], Stephanie Le Gras [d], Ludovica Cotellessa [e], Charles Decraene [a,b], Johanne Gambi [a,b], Rafael Alcala-Vida [a,b], Muthusamy Eswaramoorthy [f], Luc Buée [g,h], Jean-Christophe Cassel [a,b], Paolo Giacobini [e], David Blum [g,h], Karine Merienne [a,b], Tapas K. Kundu [c], Anne-Laurence Boutillier [a,b,*,2]

[a] University of Strasbourg, Laboratoire de Neuroscience Cognitives et Adaptatives (LNCA), Strasbourg F-67000, France
[b] CNRS, UMR7364 - Laboratoire de Neuroscience Cognitives et Adaptatives (LNCA), Strasbourg F-67000, France
[c] Transcription and Disease Laboratory, Molecular Biology and Genetics Unit, Jawaharlal Nehru Centre for Advanced Scientific Research (JNCASR), Bangalore, India
[d] University of Strasbourg, CNRS UMR7104, Inserm U1258 - GenomEast Platform – IGBMC - Institut de Génétique et de Biologie Moléculaire et Cellulaire, F-67404 Illkirch, France
[e] University of Lille, Inserm, CHU Lille, Laboratory of Development and Plasticity of the Postnatal Brain, Lille Neuroscience & Cognition, UMR-S1172, FHU 1000 Days for Health, 59000 Lille, France
[f] Chemistry and Physics of Materials Unit, Jawaharlal Nehru Centre for Advanced Scientific Research, Bangalore, India
[g] University of Lille, Inserm, CHU Lille, UMR-S1172 LilNCog - Lille Neuroscience & Cognition, Lille, France
[h] Alzheimer and Tauopathies, LabEx DISTALZ, France

ARTICLE INFO

Keywords:
Tauopathy
Aging
Epigenetics
Histone acetylation
Cholesterol
CSP-TTK21

ABSTRACT

Aging is the main risk factor of cognitive neurodegenerative diseases such as Alzheimer's disease, with epigenome alterations as a contributing factor. Here, we compared transcriptomic/epigenomic changes in the hippocampus, modified by aging and by tauopathy, an AD-related feature. We show that the cholesterol biosynthesis pathway is severely impaired in hippocampal neurons of tauopathic but not of aged mice pointing to vulnerability of these neurons in the disease. At the epigenomic level, histone hyperacetylation was observed at neuronal enhancers associated with glutamatergic regulations only in the tauopathy. Lastly, a treatment of tau mice with the CSP-TTK21 epi-drug that restored expression of key cholesterol biosynthesis genes counteracted hyperacetylation at neuronal enhancers and restored object memory. As acetyl-CoA is the primary substrate of both pathways, these data suggest that the rate of the cholesterol biosynthesis in hippocampal neurons may trigger epigenetic-driven changes, that may compromise the functions of hippocampal neurons in pathological conditions.

1. Introduction

Alzheimer's disease (AD) is an age-dependent neurodegenerative disease and the most common cause of dementia in the elderly. The hallmarks of AD comprise the accumulation of intercellular β-amyloid plaques and intraneuronal neurofibrillary tangles, made of hyperphosphorylated Tau proteins, leading to deterioration of memory and cognitive functions. Although age-related biological mechanisms favor vulnerability to AD (Mattson, 2004; Yin et al., 2016), it is not clear which ones are common or disease-specific, especially at the epigenomic/genomic level.

A better understanding of the functional complexity of the epigenome has led to growing recognition of the role of variation in histone acetylation patterns in health and disease, with new evidence establishing the dysregulation of epigenetic mechanisms in AD. This is consistent with findings reporting that epigenetic marks, such as histone

* Corresponding authors at: University of Strasbourg, Laboratoire de Neuroscience Cognitives et Adaptatives (LNCA), Strasbourg F-67000, France.
E-mail addresses: isabel.paiva@evotec.com (I. Paiva), laurette@unistra.fr (A.-L. Boutillier).
[1] Present address: Evotec (France) SAS, Toulouse F-31036 Cedex, France
[2] **Lead contact:** Anne-Laurence Boutillier (ALB)

https://doi.org/10.1016/j.nbd.2024.106538
Received 29 December 2023; Received in revised form 18 May 2024; Accepted 20 May 2024
Available online 22 May 2024

acetylation, are modulated by learning and altered in age-related memory decline (Graff et al., 2012; Graff and Tsai, 2013; Peleg et al., 2010). Recent findings showed variable levels of histone acetylation across discrete regions involved in the onset of both tau and amyloid pathology, that also associated with gene expression changes (Marzi et al., 2018; Nativio et al., 2020). Moreover, our group reported H3 acetylation increase in frontal cortex of AD postmortem brains accompanied with a dysregulation of important epigenetic enzymes (CBP, HDAC) in both frontal cortex and hippocampal structures (Schueller et al., 2020). Histone acetylation alterations have been reported in different brain structures of several AD mouse models (Lithner et al., 2013; Stilling and Fischer, 2011). Increased histone H3 acetylation was notably associated with tau hyperphosphorylation and impaired synaptic plasticity (Li et al., 2015). Large-scale changes in H3K9ac were also found associated with tau pathology in aging and AD human brains (Klein et al., 2019). Losses of histone acetylation have been documented in AD brains as well, such as H4K16ac at the proximity of aging and AD-related genes (Nativio et al., 2018), suggesting, at the epigenomic level, a link between aging and AD. Additionally, our group reported a dramatic depletion of H2Bac in the hippocampus of the Thy-Tau22 mouse model of AD-like tauopathy, associated with early spatial memory and plasticity dysfunctions (Chatterjee et al., 2018). In all, the changes on histone acetylation levels are most likely strongly dependent on the disease stage, but also on the brain cell-type assessed, as neurons and glial cells epigenome might be regulated differently during AD progression (Gjoneska et al., 2015). Of note, at the therapeutic level, treatments aimed at counteracting loss of acetylation using histone deacetylase inhibitors (HDACi) or histone acetyltransferase (HAT) activators have shown promising results in reinstating synaptic and cognitive plasticity in mouse models of AD (Benito et al., 2015; Chatterjee et al., 2018; Schneider et al., 2013; Valor et al., 2013; Yang et al., 2017).

Building on the hypothesis that dysregulation of the epigenome is critical in the etiology and progression of AD, in this study, we aimed at establishing epigenetic/transcriptomic hippocampal signatures associated with advanced (12-month-old) AD-like tauopathy, using the Thy-Tau22 mouse model. To understand disease-specific mechanisms, we led comparative studies with a mouse model of physiological aging (18-month-old mice). Lastly, as we previously reported many positive effects of an epigenetic treatment using the histone acetyltransferase activator CSP-TTK21 (Chatterjee et al., 2013) in 8-month-old THY-Tau22 mice (Chatterjee et al., 2018), we also tested this molecule at this advanced stage of the disease.

Our results revealed a strong down-regulation of the cholesterol/mevalonate pathway-related gene expression in advanced tauopathy, associated with hyperacetylation of H3K27 at neuronal enhancers, while that was not the case in response to aging, in which neuronal enhancers were rather hypoacetylated. Further, CSP-TTK21 treatment of tauopathic mice restored neuronal expression of these cholesterol pathway-related genes, as well as the H3K27ac signature at neuronal enhancers suggesting that the rate of the cholesterol biosynthesis pathway in excitatory neurons may trigger epigenetic-driven glutamatergic exacerbation in tauopathic hippocampal neurons. Finally, treatment with CSP-TTK21 restored memory performance in tauopathic mice, pointing to cholesterol gene biosynthesis in hippocampal neurons as a therapeutic target in advanced tauopathies.

2. Results

2.1. Cholesterol biosynthesis genes are significantly decreased in tauopathy

The THY-Tau22 (Tau) mouse model displays progressive development of hippocampal tauopathy associated with neuroinflammatory processes and memory impairments. At 12 months of age, Tau mice exhibit massive accumulation of abnormal Tau conformation and phosphorylation notably in the CA1 region of dorsal hippocampus (Schindowski et al., 2006; Van der Jeugd et al., 2013). Aging was modeled by comparing 18-month-old (old) WT mice to 3-month-old (young) WT mice. First, we performed RNA-seq from dorsal hippocampal tissue of 12-month-old tauopathic and aged mice as well as their respective controls (Fig. 1A). Principal component analysis (PCA) plot was generated to assess replicates variability between groups (Fig. S1A, C). Differential expression analysis between Tau and WT mice revealed a total of 113 dysregulated genes (43 up and 70 down-regulated genes) (Fig. 1B, Fig. S1B) (Table S1). Tau mice exhibited a significant down-regulation of several genes related to cholesterol biosynthetic processes, particularly involved in the mevalonate pathway (Fig. 1C, Fig. S1E, S2A), including the 3-Hydroxy-3-Methylglutaryl-CoA Synthase 1 (*Hmgcs1*) gene that catalyzes the condensation of acetyl-CoA with acetoacetyl-CoA to form HMG-CoA, the Mevalonate Diphosphate Decarboxylase gene (*Mvd*), as well as genes encoding for downstream enzymes such as the cytochrome P450 Family 51 Subfamily A Member 1 (*Cyp51*), the Methylsterol Monooxygenase 1 (*Msmo1*) and the Squalene Epoxidase (*Sqle*) genes. We further validated some of these changes by RT-qPCR using a different cohort of animals (Fig. S2B). In addition to central genes in the cholesterol metabolism, we also found a significant decrease of 24-Dehydrocholesterol Reductase (*Dhcr24*) in Tau mice (Fig. S2B). CYP51A1 decrease was also confirmed at the protein level (Fig. S2C). In all, the 16 representing main cholesterogenic genes showed a significant decrease in Taupathic hippocampi (Fig. 1D). Importantly, the same genes were also found severely down-regulated in the hippocampus of AD patients, when analyzed from (Gao et al., 2022) (Fig. S2D). By contrast, except for a mild down-regulation of *Mvd* and *Cyp51*, most of these cholesterol genes did not show any alteration in the aging cohort (Fig. S2E), suggesting that impairment of the cholesterol pathway in 12-month-old tauopathic mice does not rely only on aging processes. Among the up-regulated genes induced by tauopathy, immune/inflammatory response was shown to be the most induced pathway at transcriptomic level (Fig. S3A), as observed previously in 8-month-old Tau mice (Chatterjee et al., 2018; Laurent et al., 2017). Concerning Aging-related transcriptomics, we found a differential regulation of 250 genes between old and young mice (Fig. 1E, Fig. S1D) (Table S2). The signature of the down-regulated genes (104) showed some genes linked to neurogenesis (Fig. 1E, Fig. S3B). Up-regulated genes (146) were mostly associated with immune response as observed in the Tau mice (Fig. 1E, Fig. S3C). Some immune related genes, such as C1qb and C1qa, the initiating proteins of the classical complement cascade, were exclusively induced in Tau hippocampi (Fig. 1F). *Ctss* (homeostatic microglia) and *Gfap* (astrocyte) expression were induced by both processes. The Complement C3 gene displayed robust increase only in the aging group (Fig. 1F). Lastly, we performed an RNA-seq study using isolated astrocytes from the whole hippocampus of WT and Tau mice at different ages (Fig. 1G). The expression of Mevalonate / Cholesterol genes was strongly down-regulated in 9-month-old astrocytes vs WT ones of the same age and vs 3-month-old astrocytes from THY-Tau22 mice, emphasizing that this pathway severely affected in tauopathic astrocytes. Notably, 9-month-old WT astrocytes also showed a significant decrease of these genes compared to 3-month-old WT astrocytes, suggesting this pathway is also impacted as mice age but to a lesser extent than that seen in Tau mice.

As it has recently been shown that astrocytes can influence the neuronal epigenomic landscape through the control of cholesterol biosynthesis in homeostatic conditions (Li et al., 2021), we further checked histone acetylation changes in the hippocampus in tauopathic conditions.

2.2. H3K27ac is specifically enriched at neuronal enhancers in an advanced tauopathic stage

We next investigated the histone acetylation signatures in advanced tauopathy. H3K27ac is a robust mark of active enhancers and promoters

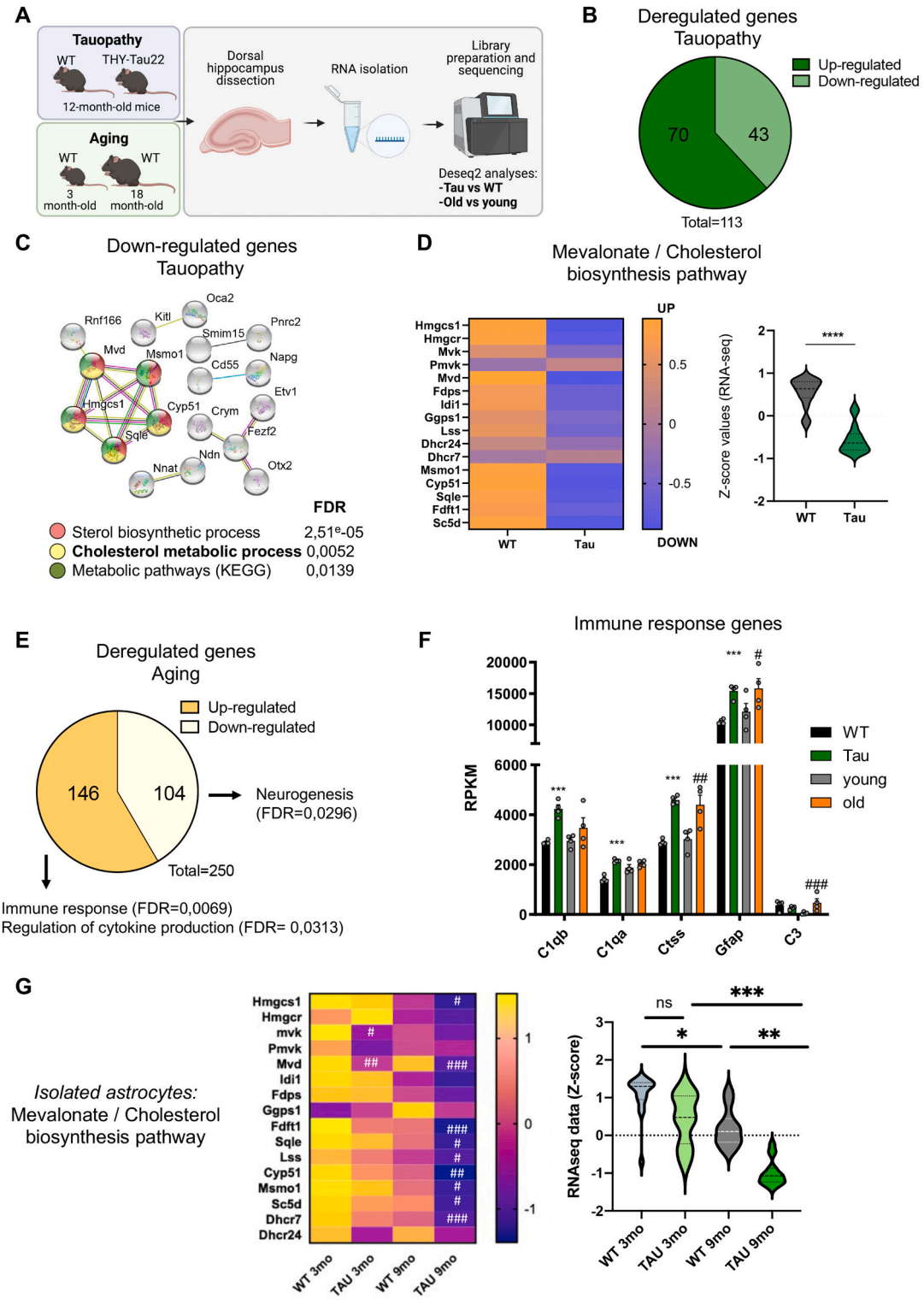

(caption on next page)

(Creyghton et al., 2010). We previously reported a depletion of this mark on neuronal enhancers in the striatum of both Aging and Huntington's disease mouse models, suggesting accelerated epigenetic aging in Huntington's disease (Alcala-Vida et al., 2021). Thus, we conducted H3K27ac ChIP-seq on 12-month-old Tau and WT bulk hippocampi. By contrast to our observation in Huntington striata, differential enrichment analysis showed a robust increase of H3K27ac in the THY-Tau22 hippocampi, with 3788 peaks enriched and 1395 depleted -regions (adjusted p-value≤0.003) (Fig. 2A) (Table S3a/3b). Gene Ontology analysis indicated that Biological processes (Fig. 2B) and Cellular component (Fig. S4A) of H3K27ac enriched genes in Tau mice were mainly associated with transport signaling pathways, such as potassium transport and axonogenesis, synapse organization, postsynaptic and synaptic membrane. The most significant KEGG pathways included axon

Fig. 1. The cholesterol biosynthesis pathway is strongly down-regulated in the hippocampus of advanced tauopathic compared to aged mice. (A) Experimental design to assess hippocampus transcriptional alterations associated with aging and tauopathy. (B) Transcriptomic results showing the deregulated genes in tauopathy, 70 up- and 43 down- regulated genes in Tau vs WT hippocampus (adjusted *p*-value ≤ 0.1) (*N* = 3–4 per group). (C) STRING network and gene ontology analysis of the down-regulated genes in tauopathy. Proteins which were not connected have been removed from the protein-protein interaction network. (D) (Left) Heatmap of the main Mevalonate/Cholesterol biosynthesis genes obtained by z-score from RNA-seq data between WT and Tau hippocampus. *Z*-score scale is represented on the right (blue, down-regulated; orange, up-regulated). (Right) Violin plot showing the overall decreased expression of these genes in tauopathic hippocampi. Student t-test. ****$p < 0.0001$. (E) Transcriptomic results showing the deregulated genes in aging, 146 up- and 104 down- regulated genes in 18 versus 3-month-old WT mice hippocampus (adjusted p-value ≤ 0.1) (N = 3–4 per group). The most significant pathways obtained by STRING are noted. (F) Expression values (RPKM) of some immune response genes obtained by RNA-seq in aging and tauopathy datasets. Statistics from DeSeq2 (p-value, RNA-seq): Tau vs WT ***$p < 0.001$; old vs young # $p < 0.05$, ## $p < 0.01$, ### $p < 0.001$. Data are represented as mean ± SEM. (G) (Left) Heatmap of the main Mevalonate/Cholesterol biosynthesis genes obtained by z-score from RNA-seq data performed in isolated astrocytes from WT and Tau mice at two different ages: 3-month-old and 9-month-old mice. *Z*-score scale is represented on the right (blue, down-regulated; yellow, up-regulated). (Right) Violin plot showing the overall decreased expression of these genes in tauopathic astrocytes. Student *t*-test when Tau is compared to WT with the same age. $^{\#}p < 0.05$; $^{\#\#}p < 0.005$; $^{\#\#\#}p < 0.001$; and Kruskal-Wallis with Dunn's multiple comparisons test as noted, *p < 0.05; **p < 0.005; ***p < 0.001; ns, nonsignificant. (For interpretation of the references to color in this figure legend, the reader is referred to the web version of this article.)

guidance, Wnt signaling, glutamatergic and GABAergic synapse as well as calcium signaling pathways (Fig. 2C). Regarding the acetylation depleted genes, we detected an overlap on axonogenesis and synapse organization-related terms (red stars, Fig. 2B, Fig. S4), but some were still specific to enriched genes. Some terms related to histone and covalent chromatin modification were exclusively linked to the depleted regions in the Tau hippocampus (blue arrows, Fig. 2B). Depleted regions showed main KEGG terms associated with transcription as well as cGMP-PKG and cAMP signaling pathways (Fig. S4B). Thus, hippocampal H3K27ac alterations emerge at late disease stages in Thy-Tau22 mice, mostly associated with enrichment in synaptic processes-related genes.

To further precise whether this epigenetic signature was neuronal, we generated ChIP-seq data using H3K27ac to identify neuronal specific regions in 12-month-old WT mice hippocampi, after neuronal (NeuN+) nuclei sorting using the fluorescence activated nuclear sorting (FANS) technique (Fig. 2D). Differential enrichment analysis between the two cell populations allowed the identification of neuronal and non-neuronal (mostly glial) regions-associated genes (Table S4). The neuronal fraction was represented by 19,084 regions (NeuN+, Fig. 2E, Fig. 5SB) and 5090 were related to non-neuronal cells (NeuN-, Fig. S5A, C). A third fraction of peaks showing no significant enrichment differences between NeuN+ and NeuN- was defined as non-specific population including 8122 regions (Fig. S5A,D). Integrated analysis of our ChIP-seq data generated on the bulk hippocampus of Thy-Tau22 and WT mice with this new cell-type-specific dataset using BedSect tool (Fig. 2F) showed that the cluster containing the largest number of overlapping regions (2089) was that containing NeuN+ and H3K27ac-enriched regions in the tauopathy model. Main biological processes associated to the corresponding genes included synaptic transmission, potassium transport, excitatory synapse as well as glutamate receptor signaling pathways (Fig. 2G). The biological processes associated with the neuronal H3K27ac depleted regions of the hippocampus of tau mice (cluster 740, Fig. 2F) indicated a preponderance of histone methylation related terms (Fig. S6A), supporting that the histone modification/methylation changes found previously in the bulk tissue analysis would be mostly associated to the neuronal population in the hippocampus of Tau mice (Fig. 2B). The non-neuronal population revealed H3K27ac enrichment (cluster 424) predominantly of genes linked to gene transcription-related processes (Fig. S6B). The H3K27ac depleted genes in the NeuN- population (cluster 189) showed association with mRNA destabilization as well as Wnt signaling and catabolic processes (Fig. S6C). Overall, these findings demonstrate a significant enrichment of H3K27ac on neuronal genes supporting the synaptic glutamatergic transmission in tauopathic mice.

2.3. H3K27ac is specifically depleted at neuronal enhancers in aging

To decipher whether tauopathy could result from an accelerated epigenetic aging, we next determined neuronal histone acetylation changes in aged mice. H3K27ac ChIP-seq were conducted in sorted neuronal nuclei (NeuN+) from hippocampus of 3-month-old (young) and 18-month-old (old) WT mice (Fig. 3A). Interestingly, we found similar numbers of enriched (1446) and depleted (1497) regions (adjusted *p*-value≤0.003) (Fig. 3B) (Table S5a/5b). By contrast to tau mice, H3K27ac-depleted neuronal genomic loci which were predominantly associated with synapse organization, neurotransmission as well as learning and memory were depleted in H3K27ac (Fig. 3C). Cellular component analysis also showed mostly synapse compartments terms associated with those regions (Fig. 3D). Moreover, KEGG analysis indicated that most of the H3K27ac-depleted regions were linked to axon guidance, glutamatergic synapse, circadian entrainment, as well as LTP and cAMP signaling-related pathways (Fig. 3E). Concerning the neuronal H3K27ac-enriched genes, cellular component analysis indicated a link to cell adhesion processes, such as collagen and extracellular matrix related terms (Fig. 3D). Thus, our results show that aging induces H3K27ac depletion at genes involved in synaptic transmission and regulation in the hippocampus, in sharp contrast with our observations made in tau mice.

2.4. H3K27ac signature on hippocampal neuronal enhancers shows opposite enrichment in aging and tauopathy

Considering that H3K27ac showed a global enrichment in hippocampal neurons of tauopathic mice, while it showed a depletion in that of aged mice, we next aimed at comparing H3K27ac signature on a specific set of neuronal enhancers. We selected these enhancers by ChIP-seq using both the active H3K27ac and the repressive H3K27me3 marks in hippocampal NeuN+ and NeuN- sorted nuclei from 5-month-old WT mice (Fig. S7A). The idea was to restrict the analysis to a set of genes associated with the neuronal identity of hippocampal cells, i.e. highly enriched in H3K27ac and depleted in H3K27me3 in the NeuN+ −enriched cell population, and vice versa in the nonneuronal (NeuN-) cell population. Bed files were aligned using SeqMINER (Ye et al., 2011) and we selected 543 genes (Fig. S7B) (Table S6), which were associated with neuronal Cellular component such as synapse part, dendrite, axon part, dendritic spine and Biological process such as modulation of synaptic transmission and ion transport-related pathways (Fig. 4A). The H3K27ac metaprofiles of these genes revealed a H3K27ac depletion in the old compared to the young mice (Fig. 4B) while tauopathic mice displayed a strong H3K27ac enrichment compared to the WT controls (Fig. 4C). Additionally, transcriptomics analysis (RNA-seq) performed from bulk dorsal hippocampus of tauopathy and aging models (Fig. 1) showed that these genes presented decreased expression in aged mice (Fig. 4D) and increased expression in the tauopathic mice (Fig. 4E). Together, these results suggest that the tauopathy condition is not just an exacerbation of aging process and develops with disease-specific dysregulations of the acetylome, significantly observable at neuronal enhancers of identity genes.

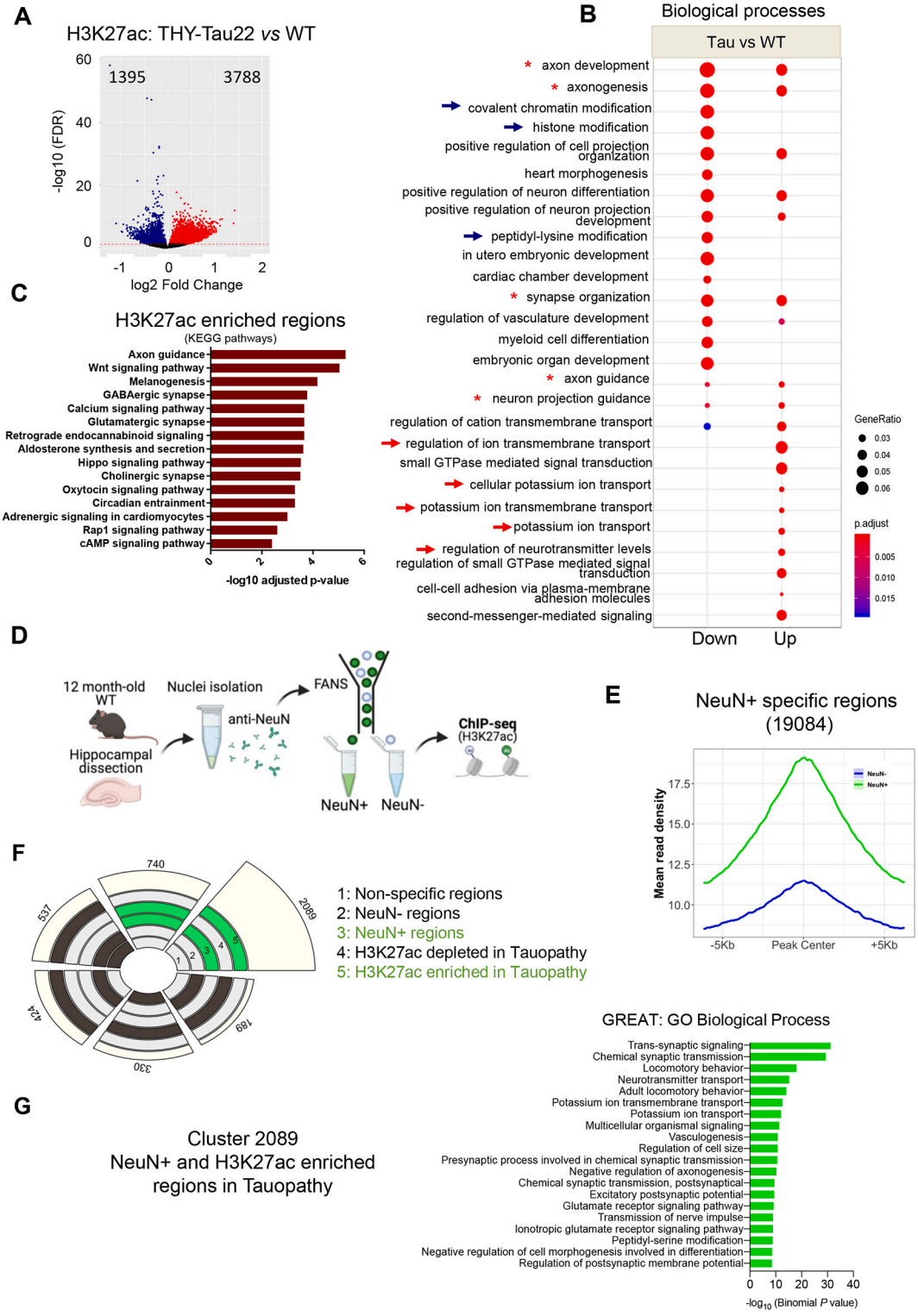

(caption on next page)

2.5. *Chronic treatment using the HAT activator CSP-TTK21 restores recognition memory and rescues cholesterol biosynthesis-related transcriptomics in advanced tauopathy*

We have previously shown that treatment with the CBP/p300 HAT activator, CSP-TTK21, was able to rescue synaptic plasticity and cognitive impairment of 8-month-old Thy-Tau22 mice (Chatterjee et al., 2018). Here, we wanted to conduct pre-clinical studies with this molecule at a later stage of the tauopathy. For that, Thy-Tau22 mice were intraperitoneally injected with CSP-TTK21 (and the control carrier molecule CSP), once every two weeks from 8 to 12 months of age. Also, a group of WT mice injected with CSP was used as a control (Fig. 5A). Memory was tested in mice using the Novel Object Recognition test. For that, the 12-month-old animal groups were subjected to a training day

Fig. 2. Synaptic transmission-related genes are enriched in H3K27ac in THY-Tau22 hippocampal neurons. (A) Volcano plot generated with the ChIP-seq H3K27ac data (bulk hippocampus) showing H3K27ac more enriched (3788) than depleted (1395) -regions in THY-Tau22 mice compared to the age-matched WT control (adjusted p-value≤0.003) ($N = 2$ biological replicates per group). (B) Biological processes generated by CusterProfiler showing the enriched and depleted regions-associated terms in THY-Tau22 mice versus WT. The statistical significance of the terms is determined by the adjusted-p-value≤0.05: red color representing highly significant terms, oppositely to the blue color. Gene Ratio, represented by the genes altered divided by the genes that belong to the respective pathway, is determined by the size of the circles. Red arrows denote ion transport terms associated to H3K27ac-enriched regions, red stars, synapse organization-related terms that are found in both enriched and depleted regions and blue arrows, chromatin modification terms associated to depleted regions (C) KEGG pathway analysis of the H3K27ac enriched regions (DAVID Functional Annotation). (D) Experimental design to define hippocampus neuronal and non-neuronal regions enriched in H3K27ac. ChIP-seq was performed on NeuN+. (neuronal) and NeuN- (non-neuronal) nuclear populations after fluorescent activated nuclei sorting (FANS) using a NeuN antibody. H3K27ac differential enrichment analysis was carried out between the two nuclear fractions in order to define neuronal and non-neuronal specific regions in age-matched hippocampi. (E) Metaprofiles generated using SeqMINER showing a greater H3K27ac enrichment on NeuN+ (green) than on NeuN- (blue) regions in that cluster, defining 19,084 NeuN+ specific regions. (F) Post-sorting analysis of the H3K27ac bulk hippocampus using BedSect tool showing biggest overlap of H3K27ac-enriched regions in tauopathy with the neuronal-specific regions (3 and 5: 2089 regions). (G) Gene ontology using GREAT, revealing that neuronal H3K27ac-enriched regions are mostly associated with synaptic transmission and glutamate receptor-related terms. (For interpretation of the references to color in this figure legend, the reader is referred to the web version of this article.)

with two similar objects (acquisition) in the open field, and one of the two objects was replaced by a new object (probe test) 24 h later (Fig. 5B, left). The amount of time taken to explore the new object provided an index of recognition memory. As expected, 12-month-old Thy-Tau22 mice spent significantly less time exploring the new object than WT mice. Excitingly, novel object recognition was fully rescued in tau mice by CSP-TTK21 treatment (Fig. 5B, right). The total time of exploration was similar among groups (Fig. S8A). Of note, nocturnal hyperactivity of tau mice was not rescued by the treatment (Fig. S8B). We then performed RNA-seq on bulk dorsal hippocampus of treated animals. Differential expression analysis between Tau CSP-TTK21 and Tau CSP showed total of 263 genes with altered expression (84 up and 179 down-regulated) (Fig. 5C). Strikingly, 40 genes previously down-regulated in Tau vs WT mice were normalized by CSP-TTK21 (Fig. S8C) and significantly associated with cholesterol biosynthesis-related pathways (Fig. 5D, Fig. S8D). Moreover, the rescue was particularly focused on the genes belonging to the cholesterol/mevalonate pathways (Fig. S2A) as CSP-TTK21 treatment produced a significant rescue of the *Hmgcs1*, *Msmo1*, *Cyp51*, *Sqle* and *Fdft1* genes as tested by RT-qPCR (Fig. 5E) and more globally of all these genes as measured by RNA-seq (Fig. 5F, Fig. S8E). Noteworthy, the treatment did not affect the inflammatory and immune response (Fig. S8F), reminiscent of what had been previously observed in these mice at 8 months of age (Chatterjee et al., 2018). Of note, up-regulated genes that were normalized by the CSP-TTK21 treatment (41 genes) were not associated with specific biological process, but included the Abca1 and Srebf1 genes, which encode proteins involved in the cholesterol and fatty acid homeostasis (Wagner et al., 2003) (Fig. S8F).

2.6. CSP-TTK21 partly rescues the neuronal H3K27ac epigenetic signature in tauopathic mice

The mevalonate/cholesterol biosynthesis pathways is strongly dependent on Acetyl-CoA availability within the cell, as it is the first substrate processed by *Hmgcs1*. Further, Acetyl-CoA is the acetyl donor for histone acetylation and changing concentrations of acetyl-CoA can restrict or promote enzymatic histone acetylation (Trefely et al., 2019). Considering the significant effect of CSP-TTK21 in restoring cholesterol biosynthesis gene expression levels, we further investigated CSP-TTK21 impact in H3K27ac levels in Tau mice. ChIP-seq experiments from bulk hippocampus of 12-month-old WT CSP, Tau CSP and Tau CSP-TTTK21 treated mice revealed that the treatment robustly decreased H3K27ac levels (56,712 regions; Adj_p ≤0.003) compared to 1978 -enriched regions (Fig. 6A) (table S7a/7b). In order to identify cell-type specific changes, we used the same NeuN+/NeuN- sorting approach and datasets mentioned in Fig. 2, to post-sort these results using BedSect tool. First of all, the greatest number of regions (15586) were neuronal (intersect 2) and showed depletion in response to treatment (intersect 7) suggesting prominent deacetylation of H3K27 in the neuronal population. Second of all, a significant overlap (shown in red, Fig. 6B) corresponded to the H3K27ac-enriched regions of tau mice that were depleted after the CSP-TTK21 and belonging to the NeuN+ population (intersect 2, 5 and 7, 1604 regions). Excitingly, these regions were mainly associated with synaptic transmission, potassium transport as well as glutamate receptor signaling pathway, suggesting that the molecule could counteract exacerbated pathways we found in the tauopathy (Fig. 6C). Furthermore, H3K27ac profile of neuronal enhancers showed that CSP-TTK21 was able to partly rescue the hyperacetylation observed in the Tau mice hippocampus (Fig. 6D). These findings raise the intriguing question of whether these changes of mevalonate/cholesterol biosynthesis pathway and histone acetylation levels, occur in the same cellular type, i.e. hippocampal neurons, making their regulation dependent on each other.

2.7. Mevalonate/cholesterol biosynthesis genes are significantly expressed by CA3/CA1 pyramidal neurons

Both astrocytes and neurons are able to synthesize cholesterol, however, with time, the capacity of neuronal de novo cholesterol biosynthesis is substantially reduced (Pfrieger and Ungerer, 2011). Yet in situ hybridization studies (Allen Brain Mouse Atlas) showed cholesterol genes are also present in neuronal layers of the adult hippocampus (Valdez et al., 2010). Thus, we further investigated which cell type could be mostly implicated in the robust dysregulation of cholesterol biosynthesis we observed using RNA-scope in situ hybridization. Hippocampal sections of 12-month-old WT mice displayed a high expression of cholesterol genes (*Msmo1*, *Sqle*, *Mvd*) mostly in the neurons (Fig. 7A). Interestingly, these genes appear to be more expressed in the pyramidal neurons of the hippocampus, presenting very high expression in the CA3 region, and their levels appeared greater than that found in astrocytes (labelled with GFAP, green). In situ RNA-scope experiments were then led in slices obtained from CSP-treated WT and TAU mice, and CSP-TTK21-treated mice (Fig. 7B). We further confirmed a decrease of *Msmo1* gene expression and its rescue by CSP-TTK21 in Tau mice in the CA3 regions, co-labelled with HuC/D marking neurons and not with S100beta marking astrocytes (Fig. 7B). This further suggests that CSP-TTK21 might play a role in neuronal cholesterol biosynthesis targeting predominantly the CA3 region. Lastly, we confirmed at the protein level the high expression of cholesterol biosynthesis proteins, such as CYP51 (Fig. S9A) and MSMO1 (Fig. S9B), in the CA3 region of the hippocampus, that appear to be reduced in Tau mice and restored by the CSP-TTK21 treatment. Overall, our study shows that enzymes from the mevalonate/cholesterol metabolism are expressed in CA3/CA1 excitatory neurons and are severely altered by the tauopathy.

3. Discussion

Our understanding of the mechanisms by which dysregulation of cholesterol metabolism contributes to the development of Alzheimer's disease remains very incomplete, as we lack studies of these mechanisms

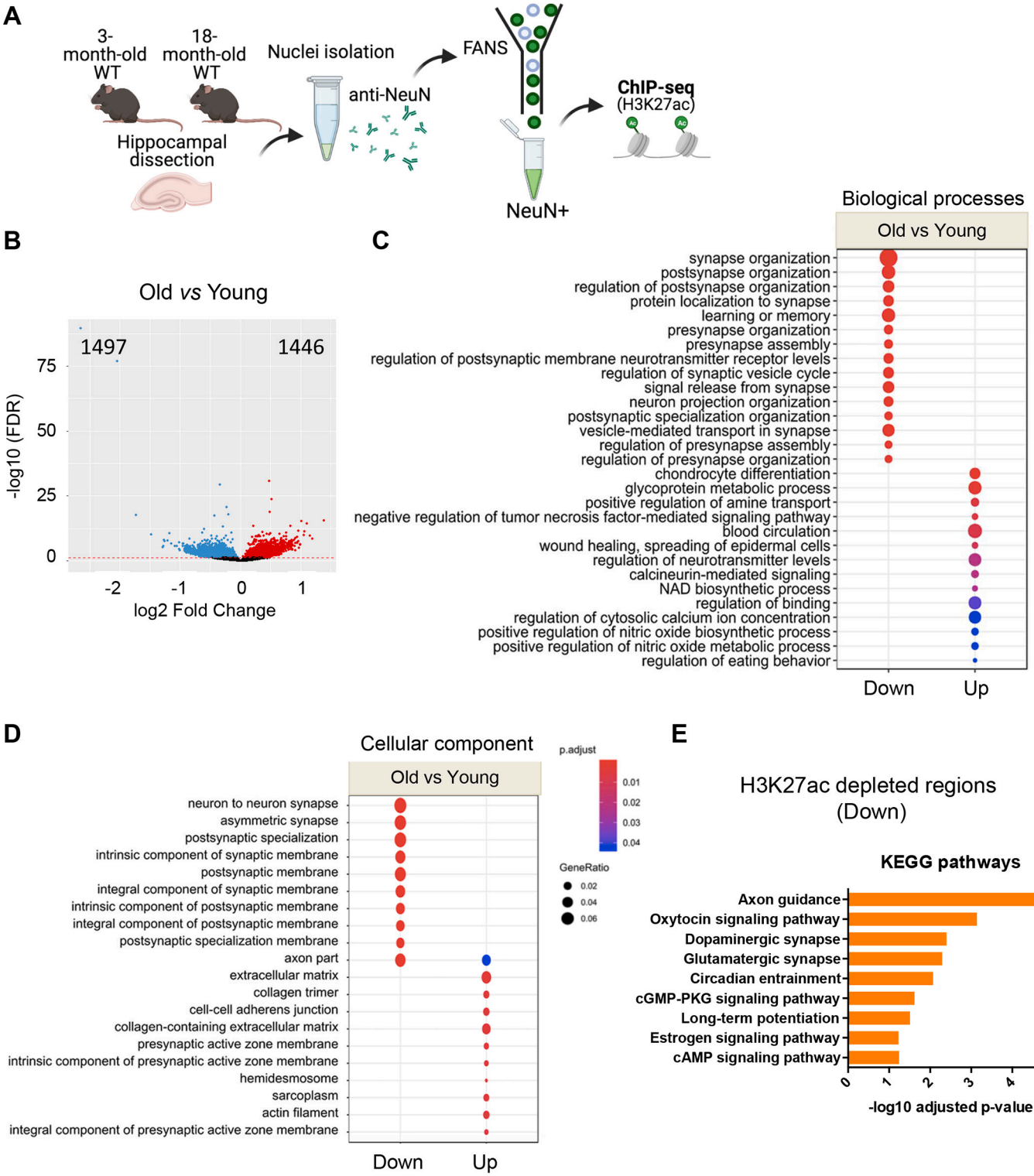

Fig. 3. Aged mice show a significantly H3K27ac depleted signature on neuronal and synaptic genes. (A) Experimental design of the aging epigenomic study. Hippocampus of 3 (young) and 18 (old) -month-old WT mice were used to perform H3K27ac ChIP-seq in the NeuN+ nuclei population (adjusted *p*-value≤0.003) (N = 2 biological replicates per group). (B) Volcano plot generated with the H3K27ac ChIP-seq data (neurons) showing H3K27ac enrichment of 1446 regions and depletion of 1497 regions. (C,D) Biological processes and Cellular component plots generated by ClusterProfiler showing the increased (Up) and depleted (Down) regions-associated terms in old versus young mice. H3K27ac depleted terms in aging are mostly associated with synapse organization. The statistical significance of the terms is determined by the adjusted-p-value (≤0.05): red color representing highly significant terms, oppositely to the blue color. Gene Ratio, represented by the genes altered divided by the genes that belong to the respective pathway, is determined by the size of the circles. (E) KEGG pathway analysis of the H3K27ac-depleted regions in aging (DAVID Functional Annotation) revealed synaptic transmission-related terms. No significant KEGG pathways were found to be statistically significant among the H3K27ac enriched terms in aging. (For interpretation of the references to color in this figure legend, the reader is referred to the web version of this article.)

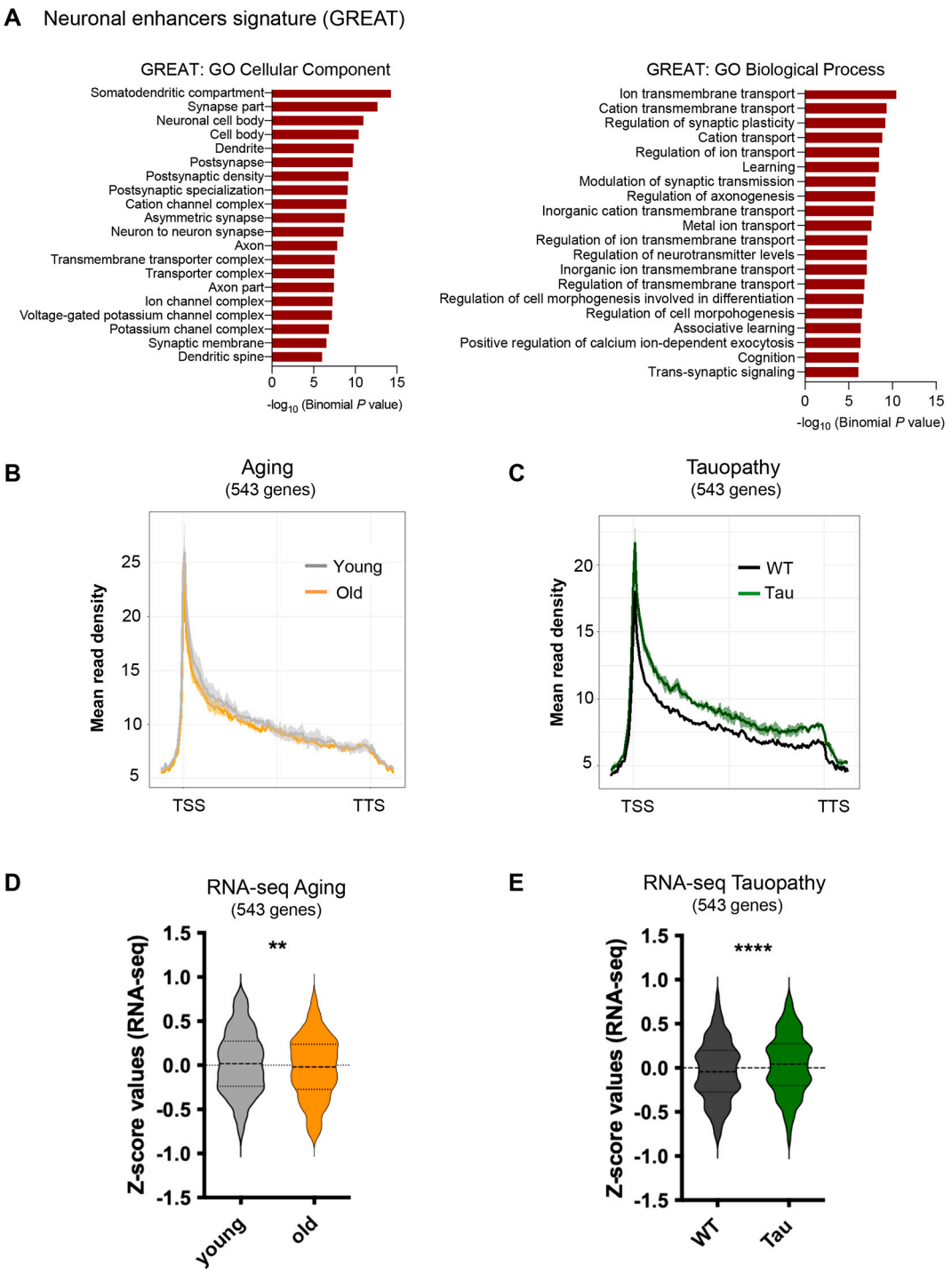

Fig. 4. Neuronal enhancers are regulated in an opposite way in aging and advanced tauopathy. (A) Gene Ontology analysis of the selection of neuronal enhancers (543 genes; Supplementary Fig. 7) using GREAT showing Cellular Component and Biological Process. (B,C) SeqMINER metaprofiles performed on these neuronal enhancers in the different contexts: old versus young mice presented H3K27ac-depleted levels in the gene body of these genes, while 12-month-old Thy-Tau22 mice displayed an enrichment of H3K27ac levels compared to the WT mice. (D,E) Z-score values of the neuronal genes expression, obtained from the RNA-seq data, showing a significant decrease of their expression levels in the aging mouse model and a significant increase in the tauopathy mouse model. Student t-test, Bonferroni correction test ** $p < 0.01$; ****$p < 0.0001$.

at the specific level of the cell. In this study, we show that the cholesterol biosynthesis pathway, particularly the mevalonate pathway, is severely impaired in the hippocampus of a tau transgenic mouse model. Down-regulation starts early in astrocytes and, at an advanced pathological stage, further spreads to CA neurons. Strikingly, this was associated with an overall increase of H3K27ac at neuronal genes in the hippocampus, likely driving these cells toward neuronal hyperexcitability. We further show that these cholesterogenic enzymes are abundantly expressed in CA1/CA3 neurons of the hippocampus (relative to that found in astrocytes) and their severe decreased expression in tauopathic excitatory neurons may reveal specific vulnerability of CA neurons to the pathological tauopathy progression. Additionally, this phenomenon is unlikely to be the result of physiological aging, since the expression of cholesterogenic enzymes was very modestly affected in the

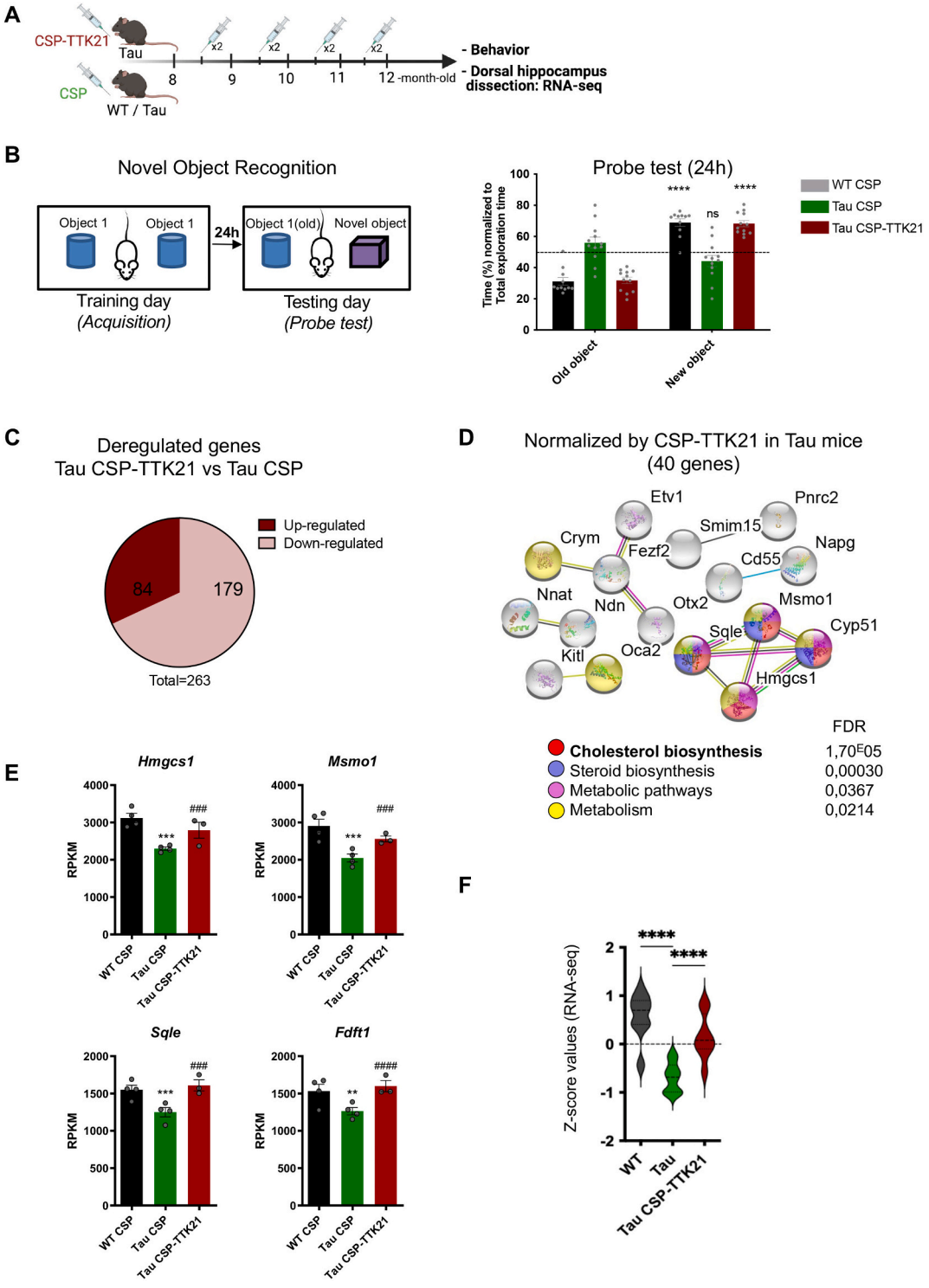

Fig. 5. The acetyltransferase activator CSP-TTK21 restores recognition memory in THY-Tau22 mice along with cholesterol biosynthesis-related transcription. (A) Timeline of the CSP (control) and CSP-TTK21 treatments. Mice were treated from 8 to 12-month-old, every two weeks, with CSP-TTK21 (500 µg/mouse/injection, $n = 11$) or CSP (vehicle, 500 µg/mouse/injection, n = 11). WT mice ($n = 12$) were injected in the same conditions with CSP. (B) Novel Object Recognition task performed with a delay of 24 h after the last training to test long term memory. Data are presented as the percentage of the time of exploration of each object (either Old, O or New, N as mentioned), normalized by the time of total exploration of both objects. Data are represented as mean ± SEM. Two-way ANOVA with Bonferroni correction test, ns, non-significant; *** when $p < 0.0001$. (C) RNA-seq was obtained from the dorsal hippocampus with $N = 4$ biological replicates/group. Comparison of CSP-TTK21-treated tauopathic mice to CSP-treated ones led to down-regulation of 179 genes and up-regulated 84 genes (p-adjusted<0.1). (D) STRING network representation of the 40 genes normalized and rescued by CSP-TTK21 showing cholesterol biosynthesis as the most significant pathway. Proteins which were not connected have been removed from the protein-protein interaction network. (E) Expression levels (RPKM) of cholesterol biosynthesis-related genes found down-regulated in the Tau mice and rescued by CSP-TTK21 treatment. Data are represented as mean ± SEM. *P*-value were obtained by Deseq2 from RNA-seq data. (F) Violin plot showing the overall decreased expression of these genes and their rescue by CSP-TTK21. One-way Anova with Bonferroni correction test. ****$p < 0.0001$.

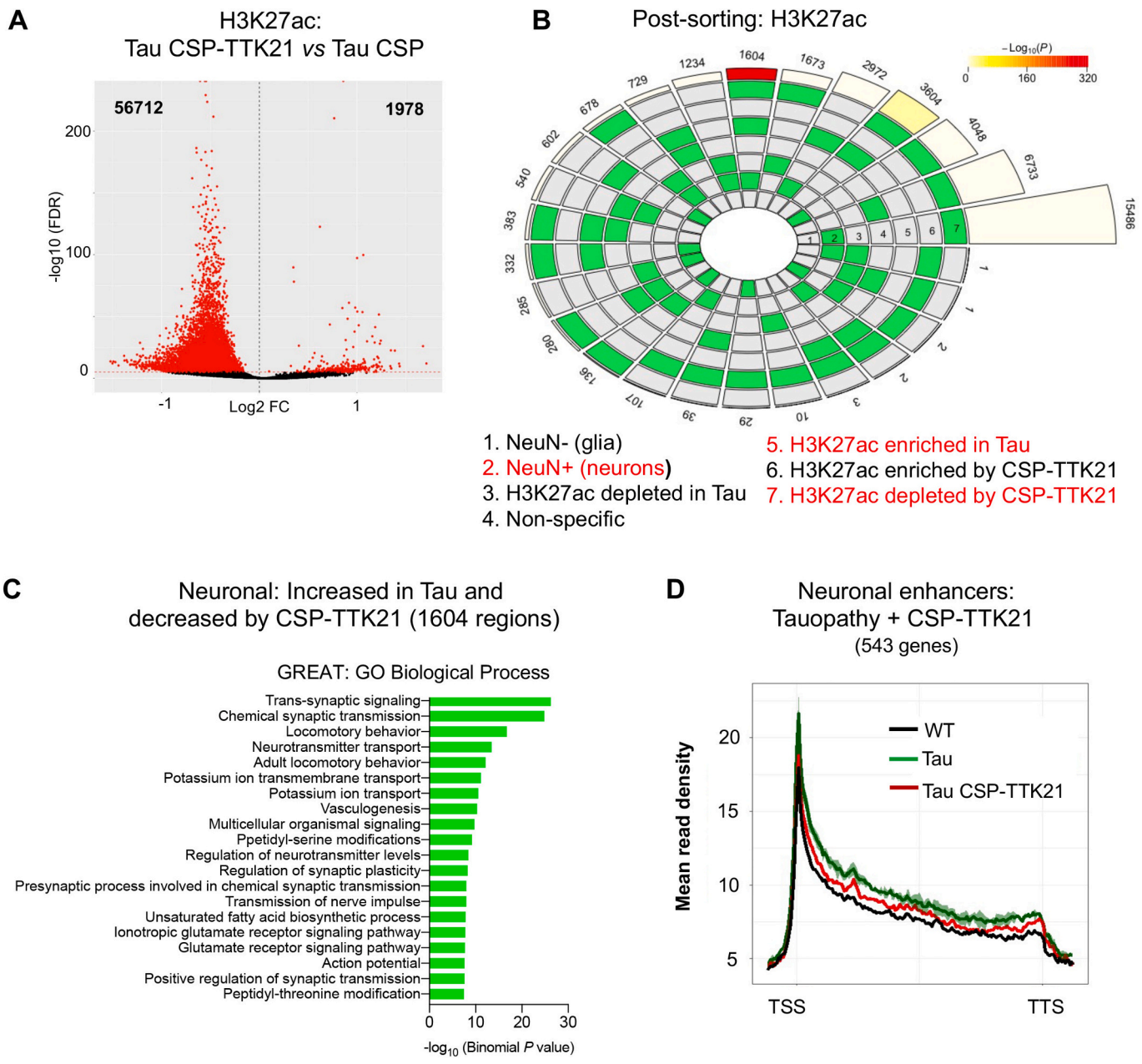

Fig. 6. CSP-TTK21 partly rescues the H3K27ac neuronal enhancer signature in Tau mice hippocampus. (A) Volcano plot of ChIP-seq data showing a global decrease of H3K27ac levels on the genome of Tau CSP-TTK21 versus Tau CSP hippocampi (bulk tissue) (adjusted p-value≤0.003). (B) Post-sorting analysis using BedSect tool (as in Fig. 2D,E) of the H3K27ac bulk hippocampus ChIP-data showing that a significant overlap between H3K27ac-enriched regions in tauopathy and decreased by CSP-TTK21 is represented by neuronal-associated regions (intersect 2, 5 and 7: 1604). (C) Gene ontology analysis (GREAT) of the neuronal H3K27ac genomic regions rescued by CSP-TTK21 showing mostly synaptic transmission and glutamate receptor -related terms. (D) Metaprofiles generated by SeqMINER performed on the selection of neuronal enhancers (543 genes; see Fig. 4A and Supplementary Fig. 6) showing partial rescue of the H3K27ac signature in Tau hippocampus after CSP-TTK21 treatment.

hippocampus of older WT mice, in which the neuronal enhancer acetylation signature was rather decreased. Lastly, these effects were prevented using the CSP-TTK21 epi-drug, which also appears to re-activate the expression of mevalonate/cholesterol-related genes and restore recognition memory of tau mice. Together, these findings highlight specific cholesterol/mevalonate pathway-dependent connection to the chromatin landscape in CA hippocampal neurons that is affected by the tauopathy, and that could account for hippocampal dysfunctions observed more generally in Alzheimer's disease. They open to several therapeutic options linked to brain cholesterol and epi-therapies.

3.1. Dysregulation of the cholesterol/mevalonate pathway in hippocampal neurons in tauopathic mice

Our results revealed a down-regulation of the cholesterol / mevalonate -related gene expression in astrocytes, starting as early as 3 months of age, that becomes prominent at 9 months of age, transcription of nearly all the key enzymes being altered. Interestingly, this down-regulation was further clearly detected in 12-month-old hippocampal neurons as well. These genes were also found globally down-regulated from RNA-seq experiments performed in the hippocampus from AD patients compared to control subjects (Gao et al., 2022), pointing to the importance of this specific pathway in AD pathological condition. AD

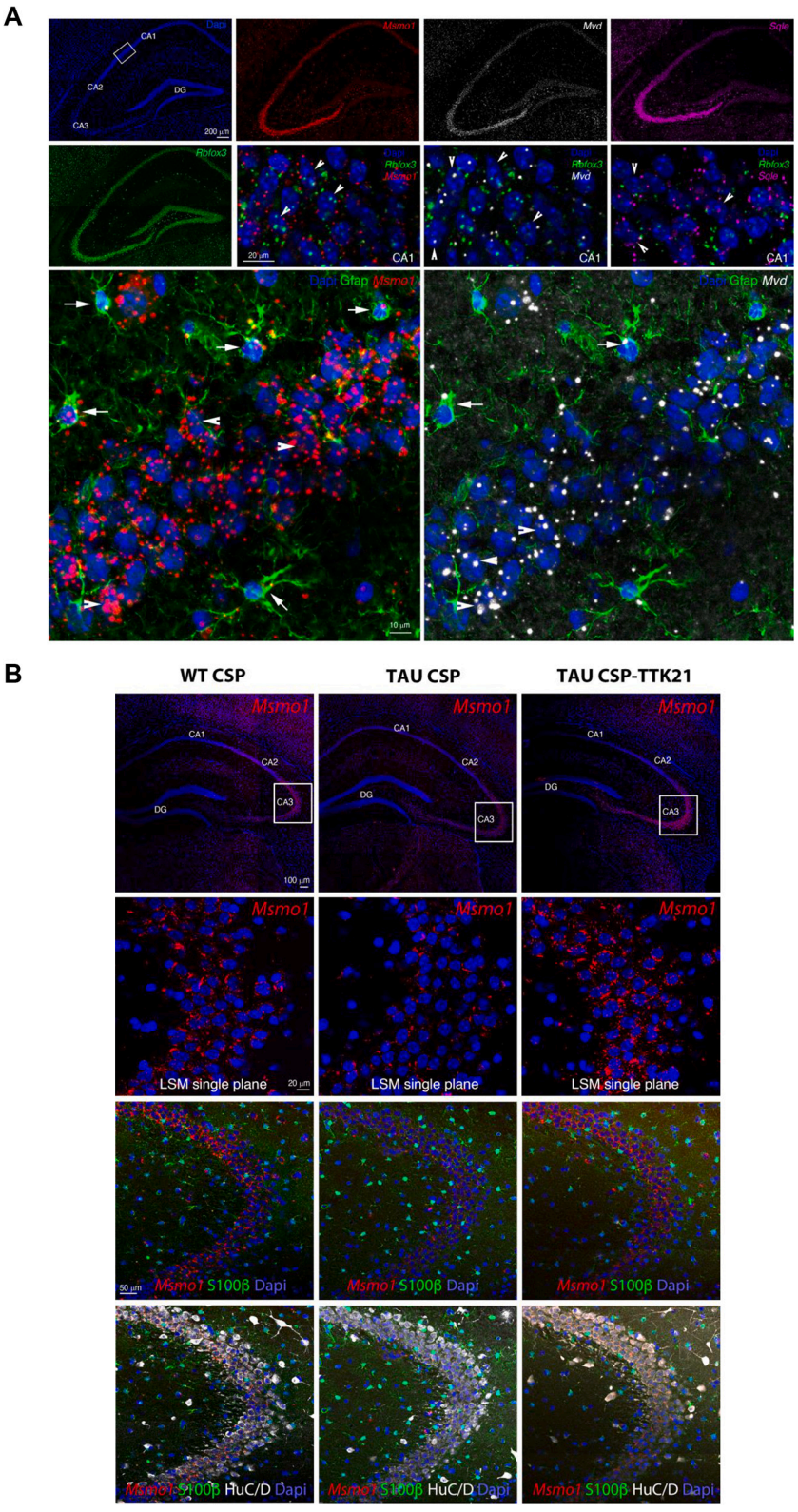

(caption on next page)

has been associated with widespread abnormalities in brain cholesterol regulations: while there is growing evidence that excess cholesterol accumulates in Alzheimer's disease (Feringa and van der Kant, 2021), it is not known whether this excess arises from cholesterol production, degradation or efflux, or how it influences the neuropathological features of Alzheimer's disease. Varma et al. (2021) reported that AD is associated with extensive dysfunctions in cholesterol biosynthesis and catabolism, showing reduced de novo cholesterol biosynthesis in response to impaired enzymatic cholesterol catabolism and efflux to maintain brain cholesterol levels in AD (Varma et al., 2021). However,

Fig. 7. Mevalonate/Cholesterol biosynthesis-related genes transcripts show significant neuronal localization, additionally to astrocytic localization in the hippocampus. (A) Upper panels: RNA-scope in situ hybridization experiments using cholesterol biosynthesis-related genes specific probes (*Msmo1*, red; *Mvd*, white; *Sqle*, purple) in 12-month-old WT mice. Co-localization of cholesterol biosynthesis-related genes with a probe targeted to *Rbfox3* transcripts (neuronal marker, green) reveals high expression of these genes in CA1 hippocampal neurons (open white arrows). Lower panels: Co-staining by immunohistochemistry using an antibody targeted to GFAP (astrocyte marker) showing that these cholesterol genes are also expressed in astrocytes (white arrows) although in less abundance compared to their observed presence in neurons (open white arrows). (B) RNA-scope in situ hybridization images showing mRNA transcripts of *Msmo1* (red) in the hippocampus of the 3 conditions (WT CSP, TAU CSP and TAU CSP-TT21) as noted. Lower panels focus on in the CA3 region of the hippocampus that display more abundant *Msmo1* levels. A co-immunostaining performed with the neuronal HuC/D (white) and astrocytic S100B (green) markers showing that *Msmo1* transcripts co-localize predominantly with neurons in the CA3 region of the hippocampus, in which levels seem decreased in TAU CSP vs WT and increased in TAU CSP-TTK21 vs TAU CSP conditions. One replicate per condition was used. (For interpretation of the references to color in this figure legend, the reader is referred to the web version of this article.)

only few studies approached the cell-type specificity of these dysregulations. Cholesterol levels were assayed in tangle-bearing neurons using semi-quantitative fluorescence microscopy with the probe filipin, in post-mortem AD temporal isocortices (Distl et al., 2001) and in a mouse model of tauopathy (P301L htau mice) (Glockner and Ohm, 2014). Both studies reported higher cholesterol levels in NFT-bearing neurons that in adjacent tangle-free neurons. Cholesterol accumulation can result from increased synthesis or defect in its efflux. Cholesterol efflux is particular in neurons as it is operated through its hydroxylation by the neuronal-specific enzyme Cyp46a1, allowing its clearance. Several studies have reported reduced 24S-hydroxycholesterol levels in patients with advanced AD or dementia, in both plasma (Bretillon et al., 2000; Kolsch et al., 2004; Papassotiropoulos et al., 2000) and cerebrospinal fluid (CSF) (Leoni et al., 2013). Cyp46a1 levels have been shown to be reduced in the hippocampus of the Tau strain used in this study (9-month-old THY-Tau22 mice) and viral overexpression of Cyp46a1 in the hippocampus that normalized CYP46A1 and 24S-hydroxycholesterol content, re-established proper neuronal function (long-term depression and dendritic spine formation) and alleviated cognitive deficits (Burlot et al., 2015). Thus, a defect in Cyp46a1 expression as occurring in THY-Tau22 neurons, could lead to a neuronal cholesterol clearance defect, hence its accumulation. It is documented that neuronal cells regulate their cholesterol content by a feedback mechanism that balances biosynthesis, import, and excretion (Nohturfft et al., 2000). A feedback regulation would take place as a compensatory response to intra-neuronal cholesterol accumulation, and higher levels of cholesterol would induce the reduction of cholesterol / Mevalonate gene transcription then, specifically in neurons. A recent paper interestingly links gamma-secretase activity to this pathway as chronic g-secretase inhibition lowered neuronal but not glial cholesterol levels, which induced transcription of genes involved in cholesterol synthesis and transport in neurons in response to the decreased cellular content of cholesterol. These cholesterol changes were associated to synaptic dysfunctions (Essayan-Perez and Sudhof, 2023). It therefore appears that neuronal regulation of cholesterol / mevalonate pathway is an important regulator of neuronal physiology, a mechanism which has been neglected until now because under physiological condition, mature neurons do not efficiently synthesize cholesterol and rely mainly on external source of cholesterol such as de novo synthesis in glial cells, and particularly in astrocytes (Pfrieger and Ungerer, 2011). However, in situ hybridization studies have reported that some adult neurons retain the ability to synthesize cholesterol, among which hippocampal neurons (Korade et al., 2007; Valdez et al., 2010). Interestingly, Valdez et al. established a "cholesterogenic map" in the adult hippocampus using the Allan Mouse Brain Atlas and showing that neurons in the pyramidal and granule cell layers express much higher levels of mevalonate pathway genes than glia (Valdez et al., 2010). This is also what we show using RNA-scope in situ hybridization, that CA3/CA1 neurons do express several of these cholesterogenic enzymes, and these are severely impaired in THY-Tau22 mice. During disease progression, one can speculate that affected astrocytes at earlier stages may no longer be able to supply neurons with the necessary cholesterol, an event that would transiently trigger CA neurons to up-regulate their own cholesterol production, which is not a sustainable option (as it costs too much energy). At 12 months of age, hippocampal neurons from THY-Tau22 mice presenting with altered metabolism may then not have sufficient energy to support memory functions. Thus, our data suggest that vulnerability of CA hippocampal neurons to tauopathy/AD may be increased because of their inability to maintain their own energy metabolism in the long term through the cholesterol/mevalonate pathway. This fits with the fact that ApoE4 is a major genetic risk factor of AD/ tauopathies (Shi et al., 2017), as cholesterol production and transport is lowered in ApoE4 carriers (Lazar et al., 2022), an event that may also precipitate CA neurons dysfunctions with regard to their ability to maintain their own cholesterol metabolism.

3.2. *How can neuronal cholesterol metabolism contribute to acetylation changes in hippocampal neurons?*

Our results suggest a link between the epigenetic drift observed in the hippocampus of tauopathic mice and alteration of the cholesterol biosynthesis pathway, detected before the mice age. Metabolic state can regulate chromatin structure, prominently involving histone modifications (Gut and Verdin, 2013). Interestingly, dynamic interplay between histone acetylation and cellular metabolism, particularly that involving cholesterol biosynthesis, was recently found to be a key mechanism underlying metabolic control of epigenetics (Trefely et al., 2019). Strikingly, this is reminiscent of a recent study showing that neuronal epigenetic acetylation states could be reprogramed by an astrocytic ApoE-dependent regulation (Li et al., 2021). This study particularly linked increased neuronal H3K27ac status to suppression of the cholesterol biosynthesis pathway within neurons, through ApoE-regulated secretion of specific miRNAs from the astrocytes. These authors clearly show that in physiological conditions, astrocytic suppression of neuronal cholesterogenic gene transcription leads to increased nuclear histone acetylation (Li et al., 2021). By contrast our study led in the pathological condition of tauopathy, shows that the clear decrease in cholesterogenic genes transcription within hippocampal neurons correlates with increased acetylation of neuronal genes. Histone acetylation has been strongly linked to cellular metabolism because of its sensitivity to the availability of acetyl-CoA (Choudhary et al., 2014; Trefely et al., 2019). Thus, alterations in acetyl-CoA levels may act as a primary factor regulating the in situ activities of acetyl-CoA-utilizing enzymes, thereby affecting the rates of associated metabolic pathways (Pietrocola et al., 2015; Szutowicz et al., 2013; Szutowicz et al., 2017). Acetyl-CoA being the primary substrate of both synthesis of cholesterol in the cytoplasmic compartment (Miziorko, 2011) and protein acetylation in the nucleus (Wellen et al., 2009), downregulation of the cholesterol/mevalonate pathway might therefore enhance acetyl-CoA availability to increase histone acetylation as seen in the Li et al. (2021) study. Of note, the nuclear membrane appears to be entirely permeable to acetyl-CoA (Wellen et al., 2009). Thus, acetyl-CoA would function as cytoplasmic rheostat that would trigger the intensity of several pathways associated with this metabolite. In a tauopathic context, upon a severe decrease in cholesterogenic gene transcription, excess of acetyl-CoA would inappropriately promote neuronal gene hyperacetylation in CA hippocampal neurons. Using the H3K27 acetylation mark, this would be particularly visible on glutamatergic-related genes in CA excitatory neurons as it is

enriched on neuronal identity genes (Hnisz et al., 2013). Hyper-activation of this pathway in the pathological hippocampus is in line with the reported GABA/glutamate imbalance (Laurent et al., 2016) and neuronal hyperexcitability described in THY-Tau22 mice (Gomez-Murcia et al., 2020). Interestingly, we found that such alterations were going the other way around during aging, suggesting disease-specific rather than age-induced epigenetic dysfunctions occurring in tau mice. Lastly, it is noteworthy that competition for acetyl-coA might also be exacerbated by other factors such as the mitochondrial dysregulations observed in pathological conditions (Bhatia et al., 2022) or acetylation of nonhistone proteins, notably of metabolic regulators (Park et al., 2015) or of the Tau protein itself (Chakraborty et al., 2023).

3.3. Restoring cholesterogenic gene expression with CSP-TTK21 partly rescues from tauopathic damages

Strikinkly, we found that CSP-TTK21 treatment of THY-Tau22 mice re-established the expression of the neuronal cholesterogenic genes and lowered H3K27ac enrichment at neuronal enhancers in the hippocampus. On the one hand, this fits with the "rheostat" model proposed above, since restoration of cholesterol / mevalonate gene transcription lowered histone acetylation levels. On the other hand, that was unexpected as CSP-TTK21 is a CBP/p300 HAT activator molecule able to induce histone acetylation (Chatterjee et al., 2013). Indeed, we previously showed in 9-month-old THY-Tau mice that CSPTTK21 treatment increased acetylation on the CBP-target H2B in the hippocampus (Chatterjee et al., 2018). In other studies, we and others found increased H4K8ac in cultured DRG neurons treated with CSP-TTK21 (Hutson et al., 2019), as well as of H3K9ac and H3K27ac in DRG, in raphe and in layer 5 cortical neurons in CSP-TTK21-treated mice (Muller et al., 2022). So multiple histones and associated lysines can be targeted by CSP-TTK21. Notably, CBP/P300 also have nonhistone-targets (Choudhary et al., 2009) that could be targeted by the CSP-TTK21 molecule. Of particular interest is the transcriptional activity of SREBPs, which is dependent on both CBP and P300 coactivators and SREBPs were shown to be acetylated by their intrinsic acetyltransferase activity (Giandomenico et al., 2003). So, we cannot exclude that other histones or nonhistone proteins may have been hyperacetylated in response to our treatment in this study. Therefore, these sites might be hyperacetylated upon CSP-TTK21 treatment hence leading to increased expression of cholesterol / mevalonate genes. Increased expression of these genes may lead to the capture of acetyl-CoA for cholesterol biosynthesis hence limiting its availability for H3K27 acetylation.

It is worth adding that CBP/P300 directly drive transcription of some cholesterol related genes, as e.g. enzymes from the mevalonate / cholesterol enzymes *Hmgcs1* and *Dhcr24*, the sterol responsive element factor *Srebf2*, the lipid transporter *Gramd1b*, a positive regulator of cholesterol biosynthesis *Sec14l2*, and the cholesterol binding protein *Sidt1*) (Bennett and Osborne, 2000; Ericsson and Edwards, 1998; Lipinski et al., 2020). So, in response to CSP-TTK21, the occupancy of CBP/P300 may be restored at cholesterol gene loci to exert a compensatory up-regulation on their transcription as we measured. Importantly, several studies indicate that CBP/P300 are present in limiting quantities for transcription in the cell (Goodman and Smolik, 2000; Vo and Goodman, 2001). In physiological conditions, CBP/P300 proteins maintain the excitatory neuron identity through the regulation of H3K27ac at cell type-specific promoter and enhancer regions (Lipinski et al., 2020). Consequently, there may be a potential titration of CBP/P300 proteins either on cholesterol gene loci or on neuronal promoter/enhancers of identity genes, thus targeting their acetylation ability. What would drive CBP/P300 shuttling between cholesterol-related genes and neuronal identity enhancer/promoters is however not known and remains to be identified. Importantly, treatment with CSP-TTK21 restored long-term object recognition memory in advanced tauopathic mice, suggesting that hippocampal functions were actually restored, supporting new therapeutic options targeting the mevalonate/cholesterol pathway, including with CBP/P300-targeted epi-drugs.

4. Conclusion

The findings presented in this study suggest that neuronal energy metabolism involving the rate of cholesterol / mevalonate gene transcription may be a crucial sensor in hippocampal neurons through the regulation of acetyl-CoA availability. In tauopathic conditions, this pathway is early affected in astrocytes and subsequently in neurons. Reduction of cholesterol / mevalonate gene transcription rate triggers hyper-acetylation of neuronal enhancers of identity genes potentially underlying brain alterations such as e.g. hyperexcitability. Interestingly, this neuronal pathway was recently highlighted by a study showing that it is under the control of gamma-secretase activity, and that its modulation is associated with synaptic release probability, so ultimately impacts synaptic transmission (Essayan-Perez and Sudhof, 2023). In terms of therapeutic options, our results bring a proof of concept that enhancing neuronal cholesterol biosynthesis in late stage of the tauopathy might be valuable to restore cognitive function and proper hippocampal functioning. It has previously been suggested that statins, HMGCR inhibitors acting to lower blood cholesterol, might be beneficial for Alzheimer's disease prevention/treatment (Jick et al., 2000; Song et al., 2013; Wong et al., 2013). However, positive correlation between statins and AD is at best inconclusive (Power et al., 2015; Zhou et al., 2007) with FDA even indicating short-term cognitive impairment in some statin users (Dowdall, 2012). Our study cautions the therapeutic value of statins in AD, as some of the molecules can easily cross the blood brain barrier, and do not show cellular specificity. Importantly, future work is needed to further evaluate the impact of cell type-specific cholesterol metabolism in AD patients.

5. Methods

5.1. Animals

For the tauopathy study, heterozygous THY-Tau22 transgenic mice were bred on a C57BL6/J background. THY-Tau22 mice overexpress the mutant human Tau protein (G272V and P301S) under the control of a Thy1.2 promoter allowing a specific neuron expression that starts at postnatal day 6 (Schindowski et al., 2006). For astrocytic-specific RNAseq studies, 3- and 9-month-old THY-Tau22 mice were used. For other analyses (CSP-TTK21 treatments, bulk RNAseq, ChIPseq and RNAscope), 12-month-old THY-Tau22 mice were used. For the Aging study, C57BL6/J WT male mice (3-month and 18-month-old) were used for bulk RNAseq and FANS-ChIPseq. For NeuN FANS H3K27ac ChIPseq, the hippocampi of 12-month-old WT mice were used. Neuronal enhancers of identity genes were defined by H3K27ac/H3K27me3 NeuN FANS-ChIPseq performed in hippocampi of 5-month-old WT mice. Male mice have been used for the whole study. Mice were 5–6 per cage (GM500, Tecniplast) and maintained under controlled housing conditions for temperature (22 °C) and light (12-h light/dark cycle), with ad libitum access to food and water.

5.2. CSP-TTK21 chronic treatment

CSP-TTK21 is the covalent bound of a glucose-derived Carbon nanoSPhere (CSP) conjugated with a potent small molecule activator (TTK21) of p300/CBP lysine acetyltransferase. TTK21 is a code for: Transcription Tapas Kundu 21 (series number of the compounds). The CSP (control) and CSP-TTK21 molecules were synthetized and produced as described in (Chatterjee et al., 2018). The molecules were stored at —20C in several aliquots, resuspended in injectable water (2 mg/mL) and sonicated for 6–8 s. Animals were injected intraperitoneally (i.p) with the molecules at the dose of 20 mg/kg of body weight. Chronic treatment was conducted by injecting WT and THY-Tau22 mice with CSP-TTK21 or CSP every two weeks from 8 to 12-month-old.

5.3. Novel object recognition

Behavioral testing took place during the light phase. Mice were single-housed for 1 week before testing. Spontaneous object exploration tests were carried out in an open field (55 × 55 × 40 cm). The open field was evenly illuminated by two indirect halogen lights (open field center, 15 lx), and a radio gave background noise from 1.5 m away (open field center, 45 ± 5 dB). Before testing, all mice received a habituation trial of 15 min with two identical objects placed in the open field. On the second day, for the acquisition phase, mice explored two identical objects during a 10-min acquisition trial, and were returned to their home cage. Ethanol (35%) followed by water were used to clean the objects and the open field between each trial. During the testing/retention day (24 h later), one of the objects was replaced by a different one, in size, material, shape, and color. Object exploration time was recorded and defined as the nose pointing toward the object within 2 cm. Gnawing and climbing of objects were not counted as exploration time. WT CSP ($N = 11$), Tau CSP ($N = 12$), Tau CSP-TTK21 (N = 12).

5.4. Actography

Spontaneous locomotor activity, was measured during 12 h dark (night) and 12 h light (day) phases. Mice were placed individually in transparent cages (42 × 26 × 15 cm) adapted to the shelves of the testing device (eight cages/shelve). Two infrared light beams, passing through each cage, were targeted on two photocells, 2.5 cm above the cage floor level and 28 cm apart. The number of cage crossing was recorded automatically and was used to determine or score the spontaneous locomotor activity. WT CSP ($N = 8$), Tau CSP ($N = 9$), Tau CSP-TTK21(N = 9).

5.5. Astrocyte isolation from mouse hippocampus

Hippocampus of 3 and 9-month old WT and Thy-Tau22 mice were freshly dissected, chopped in HBSS and incubated in preheated buffer containing DNase and papain. Following this enzymatic digestion, the sample is further mechanically dissected with the help of Pasteur pipettes of descending diameter, filtered, and subjected to myelin removal using Myelin Removal Beads II Kit (Miltenyi Biotec). The flow-through was then incubated with the FcR Blocking Reagent (10 min at 4 °C), to block the Fc receptors and increase the specificity of the staining, and with Anti-ACSA-2 MicroBeads (10 min at 4 °C) (Anti-ACSA-2 MicroBead Kit mouse, Miltenyi Biotec), to tag ATP1B2 positive cells (astrocytes). The labelled cell suspension is loaded onto a MS Column, placed in the magnetic field of a MiniMACS separator where the magnetically labelled ACSA-2+ cells are retained within the column. The column is finally removed from the magnetic field and the cells of interest eluted from the column and quantified using the TC20 Automated Cell Counter (Bio-Rad).

5.6. RNA extraction and RNA sequencing analyses

Astrocytic RNA was extracted using the RNeasy Plus Micro Kit (Qiagen) following manufacturer's instructions. Total RNA was extracted from the dorsal hippocampal tissues using the Lipid Tissue Mini Kit (Qiagen) according to the manufacturer's instructions. RNA quality control, libraries and sequencing were performed at the GenomEast platform (IGBMC, Strasbourg). The following groups were sequenced: 3-month-old WT astrocytes ($N = 3$), 3-month-old Tau astrocytes ($N = 2$), 9-month-old WT astrocytes (N = 3), 9-month-old Tau astrocytes (N = 3), and dorsal hippocampus from 12-month-old WT CSP (N = 3), Tau CSP ($N = 4$), Tau CSP-TTK21 (N = 3), 3-month-old WT (N = 4) and 18-month-old WT (N = 4) mice.

Briefly, full length cDNAs were generated from 4 ng (project: "Old vs Young"), 1 ng (project "Tau and CSP-TTK21 treatment") or 800 pg (project "isolated astrocytes") of total RNAusing Clontech SMART-Seq v4 Ultra Low Input RNA kit for Sequencing (Takara Bio Europe, Saint Germain en Laye, France) according to manufacturer's instructions with 10 (Old vs Young) or 12 (Tau and CSP-TTK21 treatment; isolated astrocytes) cycles of PCR for cDNA amplification by Seq-Amp polymerase. Six hundreds pg of pre-amplified cDNA were then used as input for Tn5 transposon tagmentation by the Nextera XT DNA Library Preparation Kit (96 samples) (Illumina, San Diego, CA) followed by 12 cycles of library amplification. Following purification with Agencourt AMPure XP beads (Beckman-Coulter, Villepinte, France), the size and concentration of libraries were assessed by capillary electrophoreris. Sequencing was performed on the Illumina® Genome Hiseq4000 as single-end 50 base reads following Illumina's instructions. Reads corresponding to rRNA were removed using Bowtie 2 aligner v2.2.8 (Frazee et al., 2015) and remaining reads were mapped onto the mm10 assembly of *Mus musculus* genome using STAR v2.5.3a (Dobin et al., 2013). Only uniquely aligned reads were kept for further analyses. Quantification of gene expression was performed using HTSeq-count v0.6.1p1 (Anders et al., 2015) and gene annotations from Ensembl release 95 and "union" mode. Read counts were normalized across libraries with the method proposed by (Anders and Huber, 2010). Comparisons of interest were performed using the test for differential expression proposed by (Love et al., 2014) and implemented in the DESeq2 Bioconductor library (v1.16.1). For two projects ("Tau and CSP-TTK21 treatment"; "isolated astrocytes"), unwanted variation was identified with SVA and considered in the statistical model. To reduce false positive, *p*-values were adjusted by IHW method. For one project ("Old vs Young"), the p-values were adjusted for multiple testing using the Benjamini and Hochberg method (Benjamini and Hochberg, 1995).

5.7. RNA extraction and quantitative real-time PCR analysis (RT-qPCR)

Dorsal hippocampus of 12-month-old mice were harvested and snap-frozen in liquid nitrogen until use. Frozen tissues were homogenized using 1 mL of QIAzol Lysis Reagent (Qiagen, #79306) with a tissue grinding pestle and total RNA was isolated using RNeasy Lipid Tissue Mini Kit (Qiagen; Cat # 74804) following the manufacturer's instructions. cDNA was synthetized from 300 ng of total RNA using the Maxima First Strand cDNA Synthesis Kit (Thermo Scientific, #K1641) under manufacturer's recommended conditions. Real-time PCR was carried out on the T100 Thermal cycler (Bio-Rad) using the PowerUP SYBR Green Master Mix (Applied Biosystems, #A25741), data were analyzed using the 2-DDCT method (Livak and Schmittgen, 2001) and normalized to both *Polr2a* and *36b4* housekeeping gene levels. Values are expressed as relative to control, which is set at 1.

5.8. Transcriptomic analysis of the Mevalonate/Cholesterol pathway from external dataset on human AD subjects

Expression levels of 16 genes affiliated to the Mevalonate/Cholesterol biosynthesis pathway were retrieved from (Gao et al., 2022) FPKM summary dataset available at NCBI GEO under the accession number GSE184942. The provided expression profiling, by high throughput sequencing, was done in the hippocampus of post-mortem Alzheimer's disease (AD) affected ($n = 5$) and control cognitively healthy subjects (n = 5).

5.9. Western blot

Dorsal hippocampi were lysed and homogenized in 4× Laemmli buffer (Bio-rad, #1610747), with addition of 1/10 β-mercaptoethanol (Sigma-Aldrich, #444203), and mixed with sample to obtain a final 1× solution. After sonication (2 × 10 s, amplitude 40%), 10 min at 70 °C and 5 min at 100 °C heating, samples were centrifuged (14,000 *g* for 5 min) and the supernatant was frozen at −20 °C until use. Protein concentration was measured using the Qubit™ Protein Assay Kit (ThermoFisher Scientific, #Q33211). Western blot was performed as

described previously (Chatterjee et al., 2018) with antibody against CYP51A1 (Proteintech, #13431–1-AP). Secondary HRP-conjugated antibody directed against rabbit was from Jackson ImmunoResearch. Blot was revealed using an Electro chimioluminescence kit (ECL) (Bio-Rad, #1705060) and visualised through a ChemiDoc molecular imager (Bio-Rad). Results were quantified using ImageLab software (Bio-Rad).

5.10. Immunohistochemistry

Immunohistochemistry was performed from floating sections ($n = 2$ WT CSP + 3 Tau CSP + Tau CSP-TTK21). Unless otherwise indicated all steps were realized at room temperature under slow agitation. After rinsing in 1× PBS (3 × 10 min) a blocking of unspecific sites and permeabilization were peformed by incubating the sections with 5% horse serum in 0.5% Triton X-100 diluted in 1× PBS for 45 min. The brain sections were then incubated overnight at 4 °C with anti-CYP51 (13431–1-AP, Proteintech) or anti-Msmo1 (ab203587, Abcam) antibodies diluted at 1/100 in 5% horse serum and 0,05% Triton X-100 PBS solution. Slices were incubated at room temperature for 2 h and after washed with 1× PBS (3 × 10 min). Slices were further incubated with anti-rabbit antibodies (A32754, Invitrogen) for 1 h, diluted at 1/2000 in a 0,05% Triton X-100 PBS solution. After rinsing with PBS (1 × 10 min) the sections were stained with a Dapi solution diluted at 1/1000 in 1× PBS. After a last rinsing (10 min in 1× PBS) the brain sections were mounted on a dried glass slide with mowiol. Observation and image acquisitions were performed using a fluorescence microscope coupled with an ApoTome module (Zeiss).

5.11. Fluorescence activated nuclear sorting (NeuN+/NeuN-)

Cell-type specific nuclear purification was performed using fluorescent activated nuclear sorting as detailed in (Tzeplaeff et al., 2023). Tissues were dissociated mechanically using a loose dounce and then fixed with 1% PFA at RT for 10 min. Cross-linking was stopped by adding 1.67 M of glycine at RT for 5 min. Samples were centrifuged at 4 °C, 3600 *g* for 5 min and then incubated in PBS with protease inhibitors (PIC) at 4 °C for 5 min (2×). After centrifugation tissues were incubated in cell lysis buffer (10 mM HEPES pH 8, 85 mM KCL, 0,5% NP-40 in ddH2O) with PIC at 4 °C for 7 min. Pellets were collected by centrifugation at 4 °C, 5000 rpm for 20 min and resuspend in nuclei extraction buffer (0,1% SDS, 10 mM EDTA pH 8, 50 mM Tris in ddH20) with PIC at 4 °C for 7 min. Nuclei were collected after centrifugation at 4 °C, 5000 rpm for 10 min, and resuspended in PBS with PIC at 4 °C for 5 min. A last centrifugation at 4 °C, 5000 rpm for 5 min is needed to obtain a clean pellet of nuclei. After nuclei isolation, purified nuclei were resuspended in PBTB (PBS 1×, 5% BSA, 0.5% Tween-20) + 1× PIC, 3% Normal Horse Serum and stained using antibody to NeuN (1:1000, Merck Millipore). After washing, nuclei were labelled with Alexa Fluor 488 donkey anti-mouse IgG antibody (1:1500) and washed with ice-cold PBS. Immunostained nuclei were sorted using BD Aria Fusion flow cytometer (70 uM noozle), recovered in ice-cold 1× PBS, pelleted and stored at −80°C for ChIP-seq experiments.

5.12. ChIP-sequencing on bulk tissue and sorted neurons

ChIP-seq experiments from whole tissue, was performed as described in (Chatterjee et al., 2018; Paiva et al., 2022). Dorsal hippocampus was chopped by a razor blade and rapidly incubated in 1.5 mL Phosphate Buffer Saline (PBS) containing 1% formaldehyde for 10 min at room temperature (RT). To stop fixation, glycine was added (0.125 M final concentration). Dorsal hippocampi from 4 mice were pooled per sample and two biological replicates were used for the ChIP-seq. Samples were sonicated using the Diagenode Bioruptor (30 s ON-30 s OFF at High Power x 35 cycles). Sonicated chromatin was centrifuged 10 min at 14000 ×*g*, the supernatant collected and diluted 1:10 in ChIP dilution buffer (0.01% SDS, 1.1% Triton X-100, 1.2 mM EDTA, 16.7 mM Tris-Cl, pH 8.1, 167 mM NaCl). Input was generated using 10% of the volume from each sample chromatin. Supernatants were incubated overnight (4 °C) with 1/1000 primary antibody H3K27ac (ab4729), followed by protein A Dynabeads (Invitrogen) for 2 h at RT. After washes (low salt, high salt, LiCl and TE buffers), DNA-protein complexes were eluted in 300 µL Elution buffer (1% SDS, 0.1 M NaHCO3). The crosslinking was reversed (overnight at 65 °C) and the DNA was subsequently purified with RNAse (30 min, 37 °C), proteinase K (2 h, 45 °C). DNA from the immunoprecipitated and input samples was isolated using Diagenode MicroChIP DiaPure columns with 20 µL nuclease-free milliQ water in low binding tubes. ChIP samples were purified at the Genomeast Platform using Agencourt AMPure XP beads (Beckman Coulter) and quantified using Qubit (Invitrogen).

For ChIP-seq experiments from sorted NeuN+ nuclei, steps were carried as described above, except for the following ones: 500000 frozen neuronal nuclei were resuspended in 500 uL Nuclei lysis buffer (10 mM EDTA, 50 mM Tris-HCL pH 8.1, 1 mM NaBu and 1% SDS H3K27ac or 0,4%SDS for H3K27me3, in ddH2O) with PIC in a 15 mL TPX tube (Diagenode). Nuclei were sonicated using the 30 s ON-30 s OFF at High Power x 17 cycles. Supernatants were incubated overnight (4 °C) with 3 µg of H3K27ac antibody (ab4729). For NeuN+ and NeuN- ChIP-seq, 500,000 frozen nuclei were used per histone mark, 3µg of rabbit anti H3K27ac antibody (ab4729) and 5µg of rabbit anti H3K27me3 (Diagenode, C15410195) were used per immunoprecipitation.

5.13. ChIP-sequencing libraries and sequencing

ChIP-seq libraries were prepared from 2 to 10 ng of double-stranded purified DNA using the MicroPlex Library Preparation kit v2 (C05010014, Diagenode s.a., Seraing, Belgium), according to manufacturer's instructions. DNA was first repaired and yielded molecules with blunt ends. Next, stem-loop adaptors with blocked 5′ ends were ligated to the 5′ end of the genomic DNA (gDNA), leaving a nick at the 3′ end. The adaptors cannot ligate to each other and do not have single-strand tails thus non-specific background is avoided. In the final step, the 3′ ends of the gDNA were extended to complete library synthesis and Illumina compatible indexes were added through a PCR amplification (4 + 7 cycles). Amplified libraries were purified and size-selected using Agencourt AMPure XP beads (Beckman Coulter) to remove unincorporated primers and other reagents. Prior to analyses, DNA libraries were checked for quality and quantified using a 2100 Bioanalyzer (Agilent). The libraries were loaded in the flowcell at 8 pM concentration, and clusters were generated using the Cbot and sequenced using the Illumina HiSeq 4000 technology as single-end 50 base reads following Illumina's instructions. Image analysis and base calling were performed using RTA and CASAVA.

5.14. ChIP-seq analysis

Reads were mapped onto Mouse reference assembly GRCm38/mm10 using Bowtie 1.0.0. aligner (Langmead et al., 2009). Mapped reads aligned along the repeated elements within the mouse genome were removed by using RepeatSoaker tools (Dozmorov et al., 2015). Then, mapped reads for ChIPseq biological replicates ($N = 2$) were merged in one new bam file for each experimental condition. Peak detection and differential enrichment were performed using the tool SICER-df included in the software SICER v1.1 (Xu et al., 2014; Zang et al., 2009) with the following parameters: window size: 200, Gap size: 1000, *e* value: 0.003, False Discovery Rate: 0.003.

Neuronal- vs glial-specific H3K27ac-enriched regions were selected using log2FC > 0.5; Adjusted p value <0.003. For Tauopathy post-sorting analysis, neuronal- and glial-specific H3K27ac-enriched regions were intersected with H3K27ac regions differentially enriched in 12-month-old Tau vs WT mice using the BedSect tool (Mishra et al., 2020).

5.15. Gene ontology analysis

ClusterProfiler package from Bioconductor was used for gene ontology analysis to compare datasets (Yu et al., 2012). List of genes for multiple comparisons were provided as input and enriched Biological Processes terms and Cellular components were identified (FDR <0.05). Significant biological processes were plotted with a dot size proportional to the gene ratio identified for each term and color scale according to its statistical significance. Additionally, GO analysis of seqMINER generated clusters was performed using GREAT (McLean et al., 2010). Independent GO analysis was performed using DAVID Functional Annotation (Benjamini<0.05) (Huang da et al., 2009). STRING was used for gene network analysis and gene ontology using default parameters (von Mering et al., 2003).

5.16. Multiplex fluorescence in situ hybridization combined with immunofluorescence

FISH was performed on fresh-frozen mouse brain sections (cryosectioned at 16 μm) using the RNAscope Multiplex Fluorescent Kit v2 according to the manufacturer's protocol (Advanced Cell Diagnostics). Specific probes were used to detect *Msmo1* (#810561-C2), *Mvd* (#1005611-C3), *Sqle* (#1005601-C2), *Rbfox3* (#313311-C1) mRNAs. Hybridization with a probe against the *Bacillus subtilis* dihydrodipicolinate reductase (dapB) gene (#320871) was used as a negative control and 3-Plex Positive (#320861) as positive control. Immunofluorescence against GFAP was performed, after RNAscope staining, as reported above. The sections were incubated at 4 °C overnight with an anti-GFAP antibody (Rabbit, DAKO, #Z0334, dilution 1:100) anti-S100β antibody (Rabbit, DAKO, #IR50461–2, Ready-to-use), and anti-HuC/D antibody (Mouse, Thermo Fisher, #A-21271, dilution 1:100), diluted in 0.1 M PBS containing 0.3% Triton X-100 and 10% normal donkey serum. The sections were then washed in PBS and incubated for 2 h with an anti-mouse Alexa Fluor® 647 AffiniPure Donkey (#A31571, Invitrogen, 1:500) and with an anti-rabbit Alexa Fluor® 488 (#A21206, Invitrogen, 1:500) diluted in PBS and counterstained with DAPI nuclear staining (1:10000; Thermo Fisher Scientific, #62248). Sections were mounted using Mowiol (Millipore, # 475904) and analyzed using an LSM 710 confocal microscope (Zeiss).

5.17. Statistics

This omics study includes different statistical approaches that are detailed in the appropriate method paragraph. All analyses were performed using Prism 8 (Graphpad Software, San Diego, CA) and assessed for normality before subsequent analyses by several statistical tests. Sample sizes were chosen according to standard practice in the field. For each experiment, replicates are described in the Fig. legends. For analyses of populations normally distributed, data were compared using an unpaired two-tailed Student's *t*-test or a one-way ANOVA for multiple comparisons followed by Tukey's or Bonferroni multiple comparison post hoc test. The number of biologically independent experiments, statistical tests, sample size, age of the animals are all indicated in the main text or Fig. legends. All experimental data are indicated as mean ± SEM. The significance level was set at $p < 0.05$, or $p < 0.1$ for RNA-seq experiments. ChIP-seq and RNA-seq statistical analysis are described in the respective sections.

5.18. Study approval

Experimental protocols and animal care followed the institutional guidelines (council directive 87/848, October 19, 1987, Ministère de l'agriculture et de la Forêt, Service Vétérinaire de la Santé et de la Protection Animale) and international laws (directive 2010/63/UE, February 13, 2013, European Community) and policies. Our project has been reviewed and approved by the ethics committee of Strasbourg, France (#AL/100/107/02/13 and APAFIS#5118-2016042017216897v9). All procedures complied with European standards for the care and use of laboratory animals.

5.19. Data availability

RNA-seq and ChIP-seq datasets generated in this study are available at NCBI GEO under the following accession number: GSE246777. All other relevant data are available within the Article, Supplementary Information, or available from the corresponding authors upon request.

Funding

This work was mainly supported by a grant obtained from the Union France Alzheimer (Association France Alzheimer maladies apparentées AAP SM 2017 #1664). Part of this work performed in ALB laboratory was supported by funding from the University of Strasbourg, Centre National de la Recherche Scientifique (CNRS), Agence Nationale de la Recherche (ANR-18-CE16-0008 and ANR-22-JPWG-0002), Fondation pour la Recherche sur le Cerveau (FRC) and Fond de Dotation AFER (2020). IP was supported during 2-year by a post-doctoral fellowship obtained from Fondation pour la Recherche Médicale (FRM, SPF201909009162) and by ANR-18-CE16-0008. JS salary was in part supported by ANR-16-CE92-0031 and ANR-18-CE16-0008. RAV was supported by IDEX fellowship (University of Strasbourg). The work performed in TKK laboratory was supported by SERB J C Bose Fellowship, Department of Science and Technology (DST), Govt. of India (JBR/2020/000029). The work performed in PG laboratory was supported by Agence Nationale de la Recherche (ANR-18-CE14-0017-02).

CRediT authorship contribution statement

Isabel Paiva: Writing – review & editing, Writing – original draft, Visualization, Validation, Methodology, Investigation, Formal analysis, Data curation, Conceptualization. **Jonathan Seguin:** Writing – review & editing, Visualization, Validation, Methodology. **Iris Grgurina:** Writing – review & editing, Visualization, Validation, Investigation, Formal analysis. **Akash Kumar Singh:** Validation, Resources, Methodology. **Brigitte Cosquer:** Methodology, Formal analysis. **Damien Plassard:** Writing – review & editing, Visualization, Validation, Formal analysis. **Laura Tzeplaeff:** Writing – review & editing, Validation, Methodology, Investigation. **Stephanie Le Gras:** Writing – review & editing, Visualization, Validation, Methodology, Formal analysis. **Ludovica Cotellessa:** Writing – review & editing, Visualization, Validation, Methodology, Investigation. **Charles Decraene:** Writing – review & editing, Methodology, Data curation. **Johanne Gambi:** Visualization, Validation. **Rafael Alcala-Vida:** Methodology. **Muthusamy Eswaramoorthy:** Writing – review & editing, Resources, Methodology. **Luc Buée:** Writing – review & editing. **Jean-Christophe Cassel:** Writing – review & editing. **Paolo Giacobini:** Writing – review & editing, Visualization, Validation, Investigation, Funding acquisition. **David Blum:** Writing – review & editing, Resources. **Karine Merienne:** Writing – review & editing, Methodology. **Tapas K. Kundu:** Writing – review & editing, Validation, Resources, Methodology, Investigation, Funding acquisition. **Anne-Laurence Boutillier:** Writing – review & editing, Writing – original draft, Visualization, Validation, Supervision, Project administration, Methodology, Investigation, Funding acquisition, Formal analysis, Conceptualization.

Declaration of competing interest

The authors declare no competing interests.

Data availability

Data will be made available on request.

Acknowledgments

We thank Olivier Bildstein, Onwukanjo-Daniel Egesi, George Edomwonyi and Aminé Isik (UMR 7364, Strasbourg) for animal care. Sequencing was performed by the GenomEast Platform, a member of the France Génomique consortium (ANR-10-INBS-0009). We would like to thank Claudine Ebel and Muriel Philipps for their support in nuclei sorting at the Cytometry Platform (IGBMC, Strasbourg). We thank Dylan Zinck, Brice Bildstein and Amrita Raja Ravi Shankar for their assistance in immunohistochemistry and RT-qPCR experiments performed during their internship.

Appendix A. Supplementary data

Supplementary data to this article can be found online at https://doi.org/10.1016/j.nbd.2024.106538.

References

Alcala-Vida, R., et al., 2021. Age-related and disease locus-specific mechanisms contribute to early remodelling of chromatin structure in Huntington's disease mice. Nat. Commun. 12, 364.
Anders, S., Huber, W., 2010. Differential expression analysis for sequence count data. Genome Biol. 11, R106.
Anders, S., et al., 2015. HTSeq–a Python framework to work with high-throughput sequencing data. Bioinformatics 31, 166–169.
Benito, E., et al., 2015. HDAC inhibitor-dependent transcriptome and memory reinstatement in cognitive decline models. J. Clin. Invest. 125, 3572–3584.
Benjamini, Y., Hochberg, Y., 1995. Controlling the false discovery rate - a practical and powerful approach to multiple testing. J. R. Stat. Soc. Ser. B Stat Methodol. 57, 289–300.
Bennett, M.K., Osborne, T.F., 2000. Nutrient regulation of gene expression by the sterol regulatory element binding proteins: increased recruitment of gene-specific coregulatory factors and selective hyperacetylation of histone H3 in vivo. Proc. Natl. Acad. Sci. USA 97, 6340–6344.
Bhatia, S., et al., 2022. Mitochondrial dysfunction in Alzheimer's disease: opportunities for drug development. Curr. Neuropharmacol. 20, 675–692.
Bretillon, L., et al., 2000. Plasma levels of 24S-hydroxycholesterol in patients with neurological diseases. Neurosci. Lett. 293, 87–90.
Burlot, M.A., et al., 2015. Cholesterol 24-hydroxylase defect is implicated in memory impairments associated with Alzheimer-like tau pathology. Hum. Mol. Genet. 24, 5965–5976.
Chakraborty, P., et al., 2023. Acetylation discriminates disease-specific tau deposition. Nat. Commun. 14, 5919.
Chatterjee, S., et al., 2013. A novel activator of CBP/p300 acetyltransferases promotes neurogenesis and extends memory duration in adult mice. J. Neurosci. 33, 10698–10712.
Chatterjee, S., et al., 2018. Reinstating plasticity and memory in a tauopathy mouse model with an acetyltransferase activator. EMBO Mol. Med. 10.
Choudhary, C., et al., 2009. Lysine acetylation targets protein complexes and co-regulates major cellular functions. Science 325, 834–840.
Choudhary, C., et al., 2014. The growing landscape of lysine acetylation links metabolism and cell signalling. Nat. Rev. Mol. Cell Biol. 15, 536–550.
Creyghton, M.P., et al., 2010. Histone H3K27ac separates active from poised enhancers and predicts developmental state. Proc. Natl. Acad. Sci. USA 107, 21931–21936.
Distl, R., et al., 2001. Tangle-bearing neurons contain more free cholesterol than adjacent tangle-free neurons. Acta Neuropathol. 101, 547–554.
Dobin, A., et al., 2013. STAR: ultrafast universal RNA-seq aligner. Bioinformatics 29, 15–21.
Dowdall, M., 2012. US FDA approves important safety label changes to cholesterol-lowering statin drugs. Clin. Lipidol. 7, 132.
Dozmorov, M.G., et al., 2015. Detrimental effects of duplicate reads and low complexity regions on RNA- and ChIP-seq data. BMC Bioinformatics 16 (Suppl. 13), S10.
Ericsson, J., Edwards, P.A., 1998. CBP is required for sterol-regulated and sterol regulatory element-binding protein-regulated transcription. J. Biol. Chem. 273, 17865–17870.
Essayan-Perez, S., Sudhof, T.C., 2023. Neuronal gamma-secretase regulates lipid metabolism, linking cholesterol to synaptic dysfunction in Alzheimer's disease. Neuron 111, 3176–3194.e7.
Feringa, F.M., van der Kant, R., 2021. Cholesterol and Alzheimer's disease; from risk genes to pathological effects. Front. Aging Neurosci. 13, 690372.
Frazee, A.C., et al., 2015. Polyester: simulating RNA-seq datasets with differential transcript expression. Bioinformatics 31, 2778–2784.
Gao, Y., et al., 2022. Proteomic analysis of human hippocampal subfields provides new insights into the pathogenesis of Alzheimer's disease and the role of glial cells. Brain Pathol. 32, e13047.
Giandomenico, V., et al., 2003. Coactivator-dependent acetylation stabilizes members of the SREBP family of transcription factors. Mol. Cell. Biol. 23, 2587–2599.
Gjoneska, E., et al., 2015. Conserved epigenomic signals in mice and humans reveal immune basis of Alzheimer's disease. Nature 518, 365–369.
Glockner, F., Ohm, T.G., 2014. Tau pathology induces intraneuronal cholesterol accumulation. J. Neuropathol. Exp. Neurol. 73, 846–854.
Gomez-Murcia, V., et al., 2020. Hyperexcitability and seizures in the THY-Tau22 mouse model of tauopathy. Neurobiol. Aging 94, 265–270.
Goodman, R.H., Smolik, S., 2000. CBP/p300 in cell growth, transformation, and development. Genes Dev. 14, 1553–1577.
Graff, J., Tsai, L.H., 2013. Histone acetylation: molecular mnemonics on the chromatin. Nat. Rev. Neurosci. 14, 97–111.
Graff, J., et al., 2012. An epigenetic blockade of cognitive functions in the neurodegenerating brain. Nature 483, 222–226.
Gut, P., Verdin, E., 2013. The nexus of chromatin regulation and intermediary metabolism. Nature 502, 489–498.
Hnisz, D., Abraham, B.J., Lee, T.I., Lau, A., Saint-André, V., Sigova, A.A., Hoke, H.A., Young, R.A., 2013. Super-enhancers in the control of cell identity and disease. Cell 155 (4), 934–947.
Huang da, W., et al., 2009. Systematic and integrative analysis of large gene lists using DAVID bioinformatics resources. Nat. Protoc. 4, 44–57.
Hutson, T.H., et al., 2019. Cbp-dependent histone acetylation mediates axon regeneration induced by environmental enrichment in rodent spinal cord injury models. Sci. Transl. Med. 11.
Jick, H., et al., 2000. Statins and the risk of dementia. Lancet 356, 1627–1631.
Klein, H.U., et al., 2019. Epigenome-wide study uncovers large-scale changes in histone acetylation driven by tau pathology in aging and Alzheimer's human brains. Nat. Neurosci. 22, 37–46.
Kolsch, H., et al., 2004. Altered levels of plasma 24S- and 27-hydroxycholesterol in demented patients. Neurosci. Lett. 368, 303–308.
Korade, Z., et al., 2007. Expression and p75 neurotrophin receptor dependence of cholesterol synthetic enzymes in adult mouse brain. Neurobiol. Aging 28, 1522–1531.
Langmead, B., et al., 2009. Ultrafast and memory-efficient alignment of short DNA sequences to the human genome. Genome Biol. 10, R25.
Laurent, C., et al., 2016. A2A adenosine receptor deletion is protective in a mouse model of tauopathy. Mol. Psychiatry 21, 97–107.
Laurent, C., et al., 2017. Hippocampal T cell infiltration promotes neuroinflammation and cognitive decline in a mouse model of tauopathy. Brain 140, 184–200.
Lazar, A.N., et al., 2022. Lipid Dys-homeostasis contributes to APOE4-associated AD pathology. Cells 11.
Leoni, V., et al., 2013. Diagnostic power of 24S-hydroxycholesterol in cerebrospinal fluid: candidate marker of brain health. J. Alzheimers Dis. 36, 739–747.
Li, L., et al., 2015. Epigenetic modulation of Cdk5 contributes to memory deficiency induced by amyloid fibrils. Exp. Brain Res. 233, 165–173.
Li, X., et al., 2021. Astrocytic ApoE reprograms neuronal cholesterol metabolism and histone-acetylation-mediated memory. Neuron 109, 957–970.e8.
Lipinski, M., et al., 2020. KAT3-dependent acetylation of cell type-specific genes maintains neuronal identity in the adult mouse brain. Nat. Commun. 11, 2588.
Lithner, C.U., et al., 2013. Disruption of neocortical histone H3 homeostasis by soluble Abeta: implications for Alzheimer's disease. Neurobiol. Aging 34, 2081–2090.
Livak, K.J., Schmittgen, T.D., 2001. Analysis of relative gene expression data using real-time quantitative PCR and the 2(-Delta Delta C(T)) method. Methods 25, 402–408.
Love, M.I., et al., 2014. Moderated estimation of fold change and dispersion for RNA-seq data with DESeq2. Genome Biol. 15, 550.
Marzi, S.J., et al., 2018. A histone acetylome-wide association study of Alzheimer's disease identifies disease-associated H3K27ac differences in the entorhinal cortex. Nat. Neurosci. 21, 1618–1627.
Mattson, M.P., 2004. Pathways towards and away from Alzheimer's disease. Nature 430, 631–639.
McLean, C.Y., et al., 2010. GREAT improves functional interpretation of cis-regulatory regions. Nat. Biotechnol. 28, 495–501.
Mishra, G.P., et al., 2020. BedSect: an integrated web server application to perform intersection, visualization, and functional annotation of genomic regions from multiple datasets. Front. Genet. 11, 3.
Miziorko, H.M., 2011. Enzymes of the mevalonate pathway of isoprenoid biosynthesis. Arch. Biochem. Biophys. 505, 131–143.
Muller, F., et al., 2022. CBP/p300 activation promotes axon growth, sprouting, and synaptic plasticity in chronic experimental spinal cord injury with severe disability. PLoS Biol. 20, e3001310.
Nativio, R., et al., 2018. Dysregulation of the epigenetic landscape of normal aging in Alzheimer's disease. Nat. Neurosci. 21, 497–505.
Nativio, R., et al., 2020. An integrated multi-omics approach identifies epigenetic alterations associated with Alzheimer's disease. Nat. Genet. 52, 1024–1035.
Nohturfft, A., et al., 2000. Regulated step in cholesterol feedback localized to budding of SCAP from ER membranes. Cell 102, 315–323.
Paiva, I., et al., 2022. Caffeine intake exerts dual genome-wide effects on hippocampal metabolism and learning-dependent transcription. J. Clin. Invest. 132.
Papassotiropoulos, A., et al., 2000. Plasma 24S-hydroxycholesterol: a peripheral indicator of neuronal degeneration and potential state marker for Alzheimer's disease. Neuroreport 11, 1959–1962.
Park, J.M., et al., 2015. Role of transcription factor acetylation in the regulation of metabolic homeostasis. Protein Cell 6, 804–813.
Peleg, S., et al., 2010. Altered histone acetylation is associated with age-dependent memory impairment in mice. Science 328, 753–756.
Pfrieger, F.W., Ungerer, N., 2011. Cholesterol metabolism in neurons and astrocytes. Prog. Lipid Res. 50, 357–371.
Pietrocola, F., et al., 2015. Acetyl coenzyme a: a central metabolite and second messenger. Cell Metab. 21, 805–821.

Power, M.C., et al., 2015. Statins, cognition, and dementia-systematic review and methodological commentary. Nat. Rev. Neurol. 11, 220–229.
Schindowski, K., et al., 2006. Alzheimer's disease-like tau neuropathology leads to memory deficits and loss of functional synapses in a novel mutated tau transgenic mouse without any motor deficits. Am. J. Pathol. 169, 599–616.
Schneider, A., et al., 2013. Acetyltransferases (HATs) as targets for neurological therapeutics. Neurotherapeutics 10, 568–588.
Schueller, E., et al., 2020. Dysregulation of histone acetylation pathways in hippocampus and frontal cortex of Alzheimer's disease patients. Eur. Neuropsychopharmacol. 33, 101–116.
Shi, Y., et al., 2017. ApoE4 markedly exacerbates tau-mediated neurodegeneration in a mouse model of tauopathy. Nature 549, 523–527.
Song, Y., et al., 2013. Association of statin use with risk of dementia: a meta-analysis of prospective cohort studies. Geriatr Gerontol Int 13, 817–824.
Stilling, R.M., Fischer, A., 2011. The role of histone acetylation in age-associated memory impairment and Alzheimer's disease. Neurobiol. Learn. Mem. 96, 19–26.
Szutowicz, A., et al., 2013. Acetyl-CoA the key factor for survival or death of cholinergic neurons in course of neurodegenerative diseases. Neurochem. Res. 38, 1523–1542.
Szutowicz, A., et al., 2017. Early and late pathomechanisms in Alzheimer's disease: from zinc to amyloid-beta neurotoxicity. Neurochem. Res. 42, 891–904.
Trefely, S., et al., 2019. Crosstalk between cellular metabolism and histone acetylation. Methods Enzymol. 626, 1–21.
Tzeplaeff, L., et al., 2023. Mutant FUS induces chromatin reorganization in the hippocampus and alters memory processes. Prog. Neurobiol. 227, 102483.
Valdez, C.M., et al., 2010. Cholesterol homeostasis markers are localized to mouse hippocampal pyramidal and granule layers. Hippocampus 20, 902–905.
Valor, L.M., et al., 2013. Lysine acetyltransferases CBP and p300 as therapeutic targets in cognitive and neurodegenerative disorders. Curr. Pharm. Des. 19, 5051–5064.
Van der Jeugd, A., et al., 2013. Progressive age-related cognitive decline in tau mice. J. Alzheimers Dis. 37, 777–788.
Varma, V.R., et al., 2021. Abnormal brain cholesterol homeostasis in Alzheimer's disease-a targeted metabolomic and transcriptomic study. NPJ Aging Mech Dis. 7, 11.
Vo, N., Goodman, R.H., 2001. CREB-binding protein and p300 in transcriptional regulation. J. Biol. Chem. 276, 13505–13508.
von Mering, C., et al., 2003. STRING: a database of predicted functional associations between proteins. Nucleic Acids Res. 31, 258–261.
Wagner, B.L., et al., 2003. Promoter-specific roles for liver X receptor/corepressor complexes in the regulation of ABCA1 and SREBP1 gene expression. Mol. Cell. Biol. 23, 5780–5789.
Wellen, K.E., et al., 2009. ATP-citrate lyase links cellular metabolism to histone acetylation. Science 324, 1076–1080.
Wong, W.B., et al., 2013. Statins in the prevention of dementia and Alzheimer's disease: a meta-analysis of observational studies and an assessment of confounding. Pharmacoepidemiol. Drug Saf. 22, 345–358.
Xu, S., et al., 2014. Spatial clustering for identification of ChIP-enriched regions (SICER) to map regions of histone methylation patterns in embryonic stem cells. Methods Mol. Biol. 1150, 97–111.
Yang, S.S., et al., 2017. The development prospection of HDAC inhibitors as a potential therapeutic direction in Alzheimer's disease. Transl. Neurodegener. 6, 19.
Ye, T., et al., 2011. seqMINER: an integrated ChIP-seq data interpretation platform. Nucleic Acids Res. 39, e35.
Yin, F., et al., 2016. Energy metabolism and inflammation in brain aging and Alzheimer's disease. Free Radic. Biol. Med. 100, 108–122.
Yu, G., et al., 2012. clusterProfiler: an R package for comparing biological themes among gene clusters. OMICS 16, 284–287.
Zang, C., et al., 2009. A clustering approach for identification of enriched domains from histone modification ChIP-Seq data. Bioinformatics 25, 1952–1958.
Zhou, B., et al., 2007. Prevention and treatment of dementia or Alzheimer's disease by statins: a meta-analysis. Dement. Geriatr. Cogn. Disord. 23, 194–201.